THESIS FOR THE DEGREE OF LICENTIATE OF ENGINEERING

Multi-Gigabaud Solutions for Millimeter-wave Communication

Sining An

Microwave Electronics Laboratory
Department of Microtechnology and Nanoscience
CHALMERS UNIVERSITY OF TECHNOLOGY
Gothenburg, Sweden 2018

Multi-Gigabaud Solutions for Millimeter-wave Communication

Sining An

Chalmers University of Technology
Department of Microtechnology and Nanoscience – MC2
Microwave Electronics Laboratory
SE-412 96 Goteborg, Sweden
Phone: 46 (0) 31 772 10 00

Technical Report MC2-406
ISSN 1652-0769

Printed by Chalmers Reproservice
Gothenburg, Sweden 2018

To my family.

Abstract

With the growing number of mobile network and internet services subscriptions, faster communication will provide a better experience for users. In the next generation mobile network, the fifth generation (5G), communication data rate will achieve several Gigabits per second with ultra-low latency. The capacity enhancement of the mobile backhaul and fronthaul is a challenge. The transmission capacity can be enhanced by increasing the bandwidth, increasing the spectrum efficiency and increasing both the bandwidth and the spectrum efficiency at the same time.

Millimeter-wave frequency bands have the bandwidth in the order of GHz which provide great opportunities to realize high data rate communications. In this case, millimeter-wave frontend modules and wideband modems are needed in communication systems. In this thesis, a 40 Gbps real-time differential quadrature phase shift keying (DQPSK) modem has been presented to support high-speed communications [A]. As a complete system, it aims to work together with the D-band frontend module published in [1] providing more than 40 GHz bandwidth. In this modem, the modulator is realized in a single field programmable gate array (FPGA) and the demodulator is based on analog components.

Although millimeter-wave frequency bands could provide wide available bandwidth, it is challenging to generate high output power of the carrier signal. In addition, the transmitter needs to back off several dB in output power in order to avoid the non-linear distortion caused by power amplifiers. In this thesis, an outphasing power combining transmitter is proposed [B] to use the maximum output power of power amplifiers while maintaining the signal quality at the same time. This transmitter is demonstrated at E-band with commercially available components.

Increasing the spectrum efficiency is an additional method to enhance the transmission capacity. High order modulation signals such as quadrature amplitude modulation (QAM) signals are commonly used for this purpose. In this case, receivers usually require coherent detection in order to demodulate the signals. Limited by the sampling rate of the analog to digital converters (ADCs), the traditional digital carrier recovery methods can be only applied to a symbol rate lower than the sampling rate. A synchronous baseband receiver is proposed [C] with a carrier recovery subsystem which only requires a low-speed ADC with a sampling rate of 100 MSps.

Keywords: Millimeter-wave communication, mobile network, high data rate, high order modulation, modem, DQPSK, power amplifier, E-band, non-linear distortion, 16-QAM, power combining, outphasing, pilot, carrier recovery.

List of Publications

Appended papers

The thesis is based on the work contained in the following papers:

[A] **S. An**, J. Chen, Z. He, S. Wang and H. Zirath, "A 40 Gbps DQPSK modem for millimeter-wave communications," *2015 Asia-Pacific Microwave Conference (APMC)*, Nanjing, 2015, pp. 1-3.

[B] **S. An**, Z. S. He, J. Chen, Y. Li and H. Zirath, "An 8 Gbps E-band QAM transmitter using symbol-based outphasing power combining technique," *2017 IEEE International Symposium on Radio-Frequency Integration Technology (RFIT)*, Seoul, 2017, pp. 150-152.

[C] **S. An**, Z. He, J. Chen, H. Han, H. Zirath, “A synchronous baseband receiver for high data rate millimeter-wave communication systems,” submitted to *IEEE Microwave and Wireless Components Letters*.

Abbreviations

2/3/4/5G	Second/Third/Fourth/Fifth generation of mobile communications technology
AC	Alternating current
ADC	Analog to digital converter
AM-AM	Amplitude to amplitude
AM-PM	Amplitude to phase
APP	Application
ASK	Amplitude shift keying
ATM	Automated teller machine
AWG	Arbitrary waveform generator
AWGN	Additive white Gaussian noise
BER	Bit error rate
BERT	Bit error rate tester
BPF	Bandpass filter
BPSK	Binary phase shift keying
CR	Carrier recovery
CW	Continuous wave
DAC	Digital to analog converter
DBPSK	Differential binary phase shift keying
DC	Direct current
DeMUX	De-serializing
DPSK	Differential phase shift keying
DQPSK	Differential quadrature phase shift keying
DSP	Digital signal processing
EVM	Error vector magnitude
FPGA	Field programmable gate array
GPRS	General Packet radio services
HD	High-definition
IF	Intermediate frequency
ISI	Inter-symbol interference
LO	Local oscillator
LPF	Low pass filter
LTE	Long-term evolution
MIMO	Multiple input and multiple output
Modem	Modulator and demodulator
MUX	Serializing

NCO	Numerical controlled oscillator
OOK	On-off keying
PAM	Pulse amplitude modulation
PAPR	Peak-to-average power ratio
PLL	Phase-locked loop
PPG	Pulse pattern generator
PRBS	Pseudo-random binary sequence
PSPR	Pilot-to-signal power ratio
P_{1dB}	1 dB compression point
QAM	Quadrature amplitude modulation
QPSK	Quadrature phase shift keying
RAN	Radio access network
RF	Radio frequency
RX	Receiver
SAW	Surface acoustic wave
SNR	Signal-to-noise ratio
TX	Transmitter
VSA	Vector Signal Analysis
WG	Waveguide
XOR	Exclusive-OR

Contents

Chapter 1

Introduction

1.1 Background

With the development of communication technology, the daily life around us becomes more and more convenient. It is nothing but normal for us to shop online, chat with friends through Facetime, watch high-definition (HD) movies at home, get cash from an automated teller machine (ATM), reply an e-mail on transportations. With the help of all kinds of software applications (APPs), we are equipped with a "superpower" of controlling things at a distance. For example, only with several taps on the cell phone from the office, the vacuum at home could start cleaning, the refrigerator could report back if the vegetables inside are fresh or not and it can even give a suggested recipe for the dinner. Credit cards, metro tickets, maps, fictions, movies etc. are all put together in a single cellphone waiting for your requests at any time.

Behind all the conveniences is a massive amount of data that we generate. The data volume is increasing exponentially, and it has been shown that more data has been created in the past two years than in the entire history of human race previously. Data is growing faster than ever before. By the year 2020, about 1.7 megabytes of new information will be created every second for every person on this planet [2]. According to Ericsson mobility report of the second quarter in 2018 [3], there were 7.8 billion subscriptions of mobile service, and the global mobile penetration achieved 103 percent. The mobile broadband subscriptions reached 5.5 billion globally. The mobile data traffic grew 52 percent in the past 12 months due to the rising number of smartphone subscriptions and the expanding average data volume per subscription.

Mobile devices and internet services become an important part of our life. Generating, sharing and exchanging the digital material become not only a lifestyle but also an important skill in modern society. The digital infrastructures of different communication networks are the skeleton of our modern life. The capacity (measured by the maximum data rate) of these communication networks becomes the main bottleneck of future applications that require even higher data rate.

1.2 Mobile network evolution

The capacity of communication networks developed rapidly in the past few decades. Taking the mobile networks as an example, the first-generation network was only able to provide voice call in 1983. In the 1990s, the second generation (2G) system was introduced which started to provide multimedia message services through the digital cellular systems at a speed of 64 kbps. Then the 2.5G and the 2.75G networks, the 2G technology combined with general packet radio service (GPRS), improved the data rate up to 144 kbps. Then the third generation (3G) technology was launched around the year 2000 which allows data services at a speed of 144 kbps to 384 kbps in wide coverage areas and a peak data rate of 2 Mbps in the local coverage area. The fourth generation (4G) mobile system, launched in 2012, offers voice, data services and multimedia services. The communication speed of the 4G network reaches up to 100 Mbps for quick moving devices and 1 Gbps for slow-moving or stationary devices [4-6].

The next generation mobile network, the fifth generation (5G), is expected to be launched in 2020. Compared with the 4G network, the 5G network is aiming to achieve ultra-low latency around 1 ms, significantly fast data transmission at a maximum speed of several Gbps and an increase of the total capacity by a thousand times. Besides providing the traditional mobile network and internet services, the 5G network has a great opportunity to open up new dimensions of use cases. The enhanced mobile broadband services will provide immersive experiences with augmented reality and virtual reality. Interactive, multiple-participant applications and remote applications will also be developed with 5G network. In the automotive areas, real-time vehicle to vehicle and vehicle to infrastructure communications and interactions will be achieved with the help of 5G technologies. In the healthcare areas, the high-speed connection between doctors and patients can minimize required traveling and make the best use of healthcare resources. With the 5G network, the remote monitoring, medication and remote operations will be enabled. In the manufacturing areas, 5G technology will permit the manufacturing industry to move from process automation to flow management and remote supervision, and ultimately cloud robotics and remote control. For energy and utilities, mobile broadband communications are already used extensively for metering and smart grid applications. 5G will enable sophisticated resource management and automation and increase the possibilities of machine intelligence and real-time control [7-11].

The massive data increase driven by applications brings great challenges to the radio access network (RAN). The three main transport mediums used in RAN are copper cables, optical fibers and wireless links. Copper cables have been widely used for the past 100 years. With the growing demand for high data rate communications, copper cables become obsolete due to its narrow bandwidth and short transmission distance. On the other hand, optical fibers become more and more popular for its large bandwidth and robust long-distance transmission. However, it is expensive and time-consuming to install the optical fibers in the field. As a cost-efficient and flexible alternative of the fibers, wireless communication has been earning attention recently. However, wireless technologies need to offer comparable capacity as the fibers in order to eventually take over the market. Besides these three main mediums, dielectric waveguide is another option of wires communications. It provides a wide bandwidth for communications at the cost of higher losses. It can be used for high data rate interconnections.

It shares the same modems and frontend modules with wireless communications. In today's mobile networks, the mobile backhaul is evolving with a mixture of fiber and microwave links. More than 65 percent of all radio sites will be connected by microwave links in 2022 [12]. The challenges and opportunities of the high data rate communication are discussed in the next section.

1.3 Challenges and opportunities for high data rate communications

The data rate in a communication system can be described using the formula below according to [13]

$$W = K \times M, \tag{1.1a}$$

$$M = log_2(m). \tag{1.1b}$$

Where *W* is the achievable data rate with the unit of bit per second (bps). *K* is the symbol rate, namely, how many symbols are sent in each second. *m*, the modulation order, represents the total number of different symbols. *M* indicates how many bits that one symbol could represent, which is also referred to as the spectrum efficiency. As an example, a 128-QAM signal can represent 7 bits in each symbol. For example, if a 5 Gbaud 16-QAM signal is transmitted through a communication system, the data rate of this system is 5×4=20 Gbit/s. Therefore, there are two methods to increase the data rate: increasing the symbol rate or increasing the modulation order, where the modulation order also indicates the spectrum efficiency.

According to the Shannon theorem [14], the capacity of a noisy communication channel is a function of available bandwidth and the signal to noise power ratio

$$C = Blog_2(1 + \frac{S}{N}). \tag{1.2}$$

Where *C* represents the channel capacity, *B* is the bandwidth, *S* and *N* represent the power of the signal and the noise, respectively.

Shannon theorem sets a maximum limit of the data rate that a given channel can support for error-free transmission. The bandwidth limits the maximum symbol rate while the signal to noise ratio (SNR) limits the modulation order as well as the spectrum efficiency. As a result, either larger bandwidth or higher SNR is required to increase the communication data rate.

1.3.1 **High symbol rate**

In a communication system, the bandwidth of a channel determines the symbol rate that could be transmitted. In order to achieve a higher symbol rate, more bandwidth is needed. Generally, more bandwidth is available at a high carrier frequency which implies a lower relative bandwidth. However, for wireless communications, higher carrier frequency suffers more attenuation caused by both radiation loss and absorption by the atmosphere, such as Oxygen, carbon dioxide, water vapor and rain. A figure of the atmospheric attenuation at different

frequencies is shown in Fig. 1.1 [15]. There are attenuation peaks at certain frequencies which are not suitable for long-distance wireless transmission. However, these frequency bands are often allocated for short-range communications by the authorities.

The microwave bands, from 6 to 42 GHz, usually have a narrow bandwidth of several tens MHz due to the regulation, which limits the communication data rate. On the other hand, millimeter-wave bands (30 – 300 GHz) provide a great opportunity to realize high data rate communications. Millimeter-wave bands such as E-band (71-76 GHz, 81-86 GHz), D-band (110-170 GHz) and G-band (140-220 GHz) provide sufficient bandwidth to support tens of Gbps wireless communications. For the case of interconnection via dielectric waveguides system can even utilize full waveguide (WG) band without any constraints from frequency regulation.

The communication channel includes not only the medium that radio wave propagates but also all the components in this system. Highly integrated transceivers have been demonstrated in D-band for more than 40 GHz bandwidth [1]. Similar work has been also demonstrated in G-band, where the transmitter and receiver modules have a 3-dB RF bandwidth up to 35 GHz at a center frequency of 240 GHz [16]. The NTT device technology lab has designed a 300 GHz transceiver with 30 GHz bandwidth based on InP-HEMT technology [17]. In addition to wideband transceivers, realizing wideband modulators and demodulators (modems) is another challenge. To address this challenge, a 40 Gbps DQPSK modem is presented in paper [A].

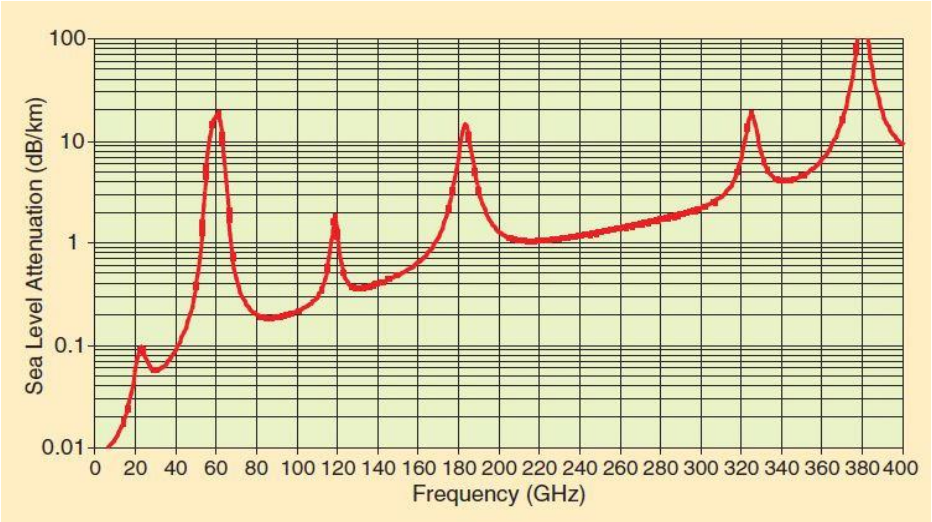

Fig. 1.1 Atmospheric attenuation at different frequencies. [15]

1.3.2 **High spectrum efficiency**

For a given bandwidth, improving the spectrum efficiency by using high order modulations could further increase the transmission data rate. In practice, transmission systems with high spectrum efficiency are difficult to realize because it is not only difficult to generate a high SNR modulated signal at millimeter-wave, but also challenging to implement the real-time demodulation at the receiver side.

In Fig. 1.2, constellations for different modulation formats are shown. For a higher order modulation, the constellation points are denser, which result in smaller decision region for each symbol. Therefore, it is more vulnerable to noise and interference. Fig. 1.3 shows the theoretical bit error rate (BER) of different modulation signal under noisy channels with different Eb/N_0. Eb/N_0 is a normalized signal-to-noise ratio (SNR) measure, also known as the "SNR per bit". To keep the same BER, high modulation order signal requires a higher SNR than a low modulation order signal does. In other words, the spectrum efficiency is limited by the SNR in the channel. The atmospheric attenuation of the millimeter-wave frequency band is higher compared to frequency bands below 40 GHz. The SNR would further decrease with the distance of the transmission.

Other than that, a high order QAM signal, such as 64-QAM, have a high peak to average power ratio (PAPR) than lower order QAM signals and phase shift keying (PSK) signals. When the signal passes through a power amplifier, high order QAM signals are easily get distorted if the power amplifier doesn't operate in its linear region. The power amplifier needs to back off from the maximum output power to its linear region to avoid non-linear distortions. As a result, the mean output power of the signal with higher PAPR, such as a high order QAM signal, will be lower.

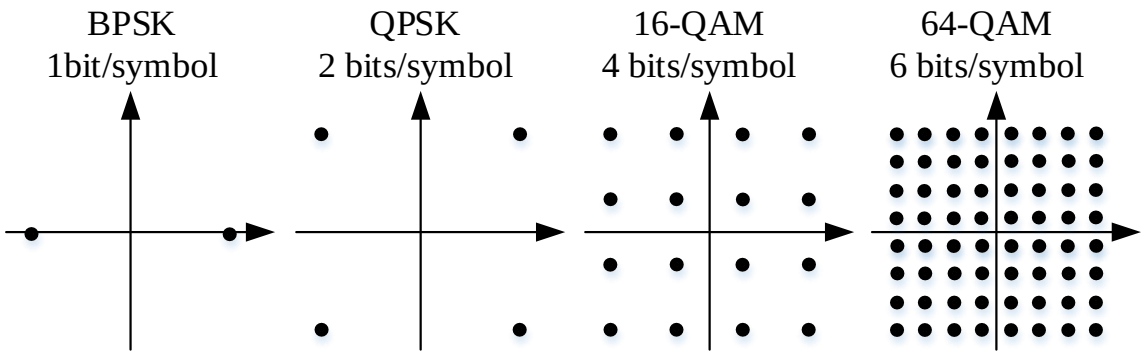

Fig. 1.2 Constellations of different modulation order signals.

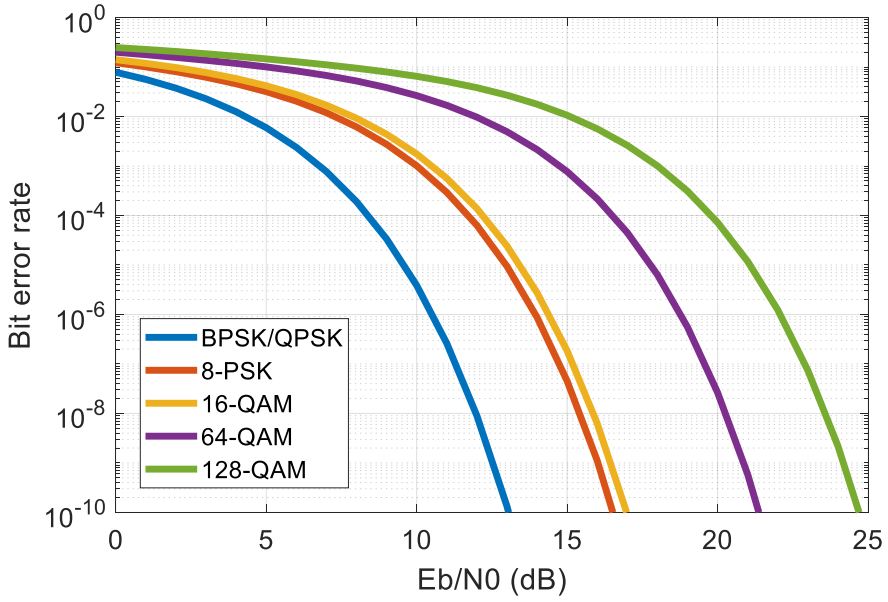

Fig. 1.3 Theoretical bit error rate as a function of signal to noise ratio per bit.

Beside the Additive White Gaussian Noise (AWGN), there is multiplicative noise in the system as well. In millimeter-wave communications, the baseband signals need to be upconverted to a millimeter-wave frequency by mixing with a carrier signal which is generated by a local oscillator (LO). When the LO signal mixes with the baseband signal, the LO noise is also multiplied with the signal, which would further deteriorate the signal quality. The LO white noise would cause the signal to suffer from both angular and amplitude noise as Fig. 1.4 shows [18]. Furthermore, it is difficult to implement a phase-locked loop (PLL) that directly generates a millimeter-wave frequency signal. The millimeter-wave LO is usually generated by a PLL with an additional multiplier. This would increase the LO noise floor by 20log(N). Compared to the lower modulation order signal, a higher order QAM signal get lower output power after amplification. In order to have a high spectrum efficiency system, the signal power at the transmitter side must be improved for a higher SNR. A QAM transmitter with symbol-based outphasing power combining technique is proposed in paper [B]. It provides a power combining solution to avoid the power back-off in amplifiers while maintaining the signal quality at the same time. As a result, more output power is obtained.

(a) (b)

Fig. 1.4 64-QAM signal constellation diagrams with (a) only multiplicative white LO noise and (b) only AWGN noise. [18]

It is also a challenge to implement a receiver for high spectrum efficient QAM modulations. For low modulation order signals, it is possible to demodulate using non-coherent detection. Such as on-off keying (OOK) and amplitude modulation (AM) signals can be demodulated by power detectors. Binary phase shift keying (BPSK) and quadrature phase shift keying (QPSK) signals can be recovered by applying differential coding to the transmitter side and differential detection at the receiver side. But for higher order QAM signals with higher spectrum efficiency, the coherent detection is inevitable at the receiver side. The carrier frequency must be recovered at the receiver side to demodulate the QAM signal. In paper [C], a synchronous baseband receiver with a carrier recovery (CR) subsystem is proposed for this purpose.

1.4 Overview of published millimeter-wave communication demonstrators

High data rate communications could be achieved by moving the carrier frequency to millimeter-waves for the larger available bandwidth of multiple GHz. A summary of published millimeter-wave transmission experiments is shown in Fig. 1.5 including spectrum efficiency and the single-channel data rate. The published results can be categorized into three groups: transmission with shared LO, where the transmitter (TX) and the receiver (RX) are sharing a

single LO source; off-line demodulation, where TX and RX use different LOs and the demodulation is implemented in off-line digital signal processing (DSP) platforms; real-time transmission, where TX and RX use different LOs and the demodulation is implemented in real-time.

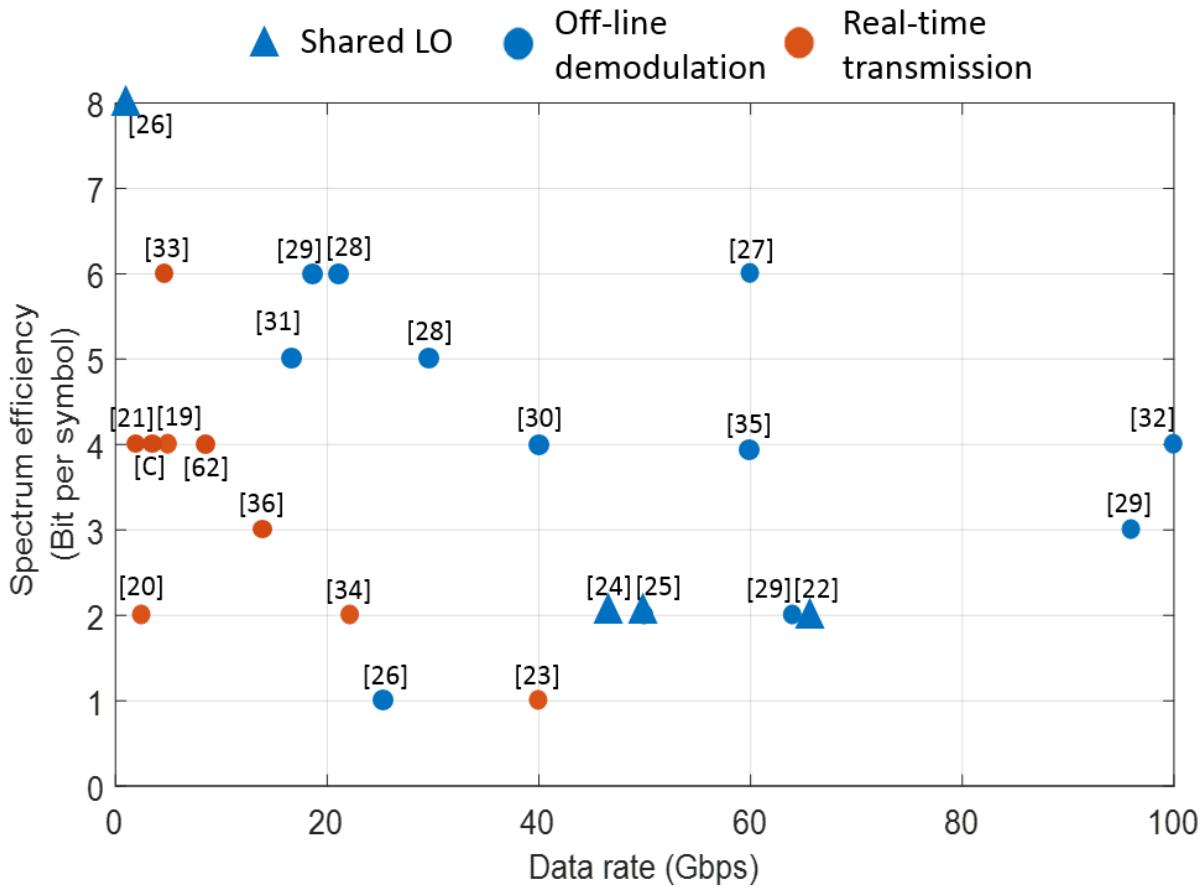

Fig. 1.5 Published single-channel millimeter-wave transmission experiment.

With a shared LO source, data transmission up to 65 Gbps has been verified [22] [24-26]. Besides, with the help of offline digital signal processing, a 64-QAM signal with data rate up to 60 Gbps has been transmitted over D-band [27]. Wireless data transmission at 240 GHz carrier frequency over a distance of 40 meters has been demonstrated with 96 Gbps 8-PSK signal [29]. A 100 Gbps wireless data transmission using 16-QAM over a distance of 2.22 meter is achieved [32]. These experiments exhibit the bandwidth potential of the transceiver chipsets.

In real-time transmission systems, lower modulation order signals such as ASK and OOK signal can be recovered by direct detection. BPSK and QPSK signals can be demodulated by using differential coding and detection. For higher order QAM signals such 16-QAM or 64-QAM, DSP platforms are commonly needed to realize carrier recovery. Normally the carrier recovery is accomplished by analyzing the received IF signal. Due to the lack of high-speed analog to digital converters, the real-time transmissions with high modulation order (higher than 16-QAM) signals in DSP platforms have only demonstrated with low data rate below 5.3 Gbps [33]. In paper [C], a real-time 4 Gbps 16-QAM transmission is accomplished with help of a carrier recovery subsystem using a low-speed ADC.

1.5 Thesis scope and outline

The thesis scope is addressed in Fig. 1.6. The first chapter introduces the background and the development of high data rate communications. In addition, the challenges and opportunities are also discussed in Chapter 1. According to the Shannon theorem, the high data rate communication can be realized by using either wide bandwidth or high modulation order signals. To utilize the wide bandwidth in millimeter-wave frequencies, a wideband modem is needed. To utilize high modulation order signals, there are some challenges to overcome. For millimeter-wave frequency signals, the SNR is limited due to low output power and high path loss, which limits the modulation order. Besides that, the synchronization in the receiver for high modulation order signals is more complicated. The carrier recovery is inevitable to achieve synchronization. In Chapter 2, a wideband modem is introduced, where the modulator is based on an FPGA and the demodulator is realized by analog components. In order to solve the problems in using high modulation order signals, solutions in both the transmitter side and the receiver side are introduced. In Chapter 3, a symbol-based outphasing power combining transmitter is illustrated to deal with the SNR and the distortion problem of QAM signals. In Chapter 4, a hardware efficient baseband receiver with a carrier recovery subsystem is presented. A real-time transmission through E-band is demonstrated. This work is presently the only modulation independent baseband receiver solution which only requires a 100 MSps ADC. Finally, the conclusion and discussions are given in Chapter 5.

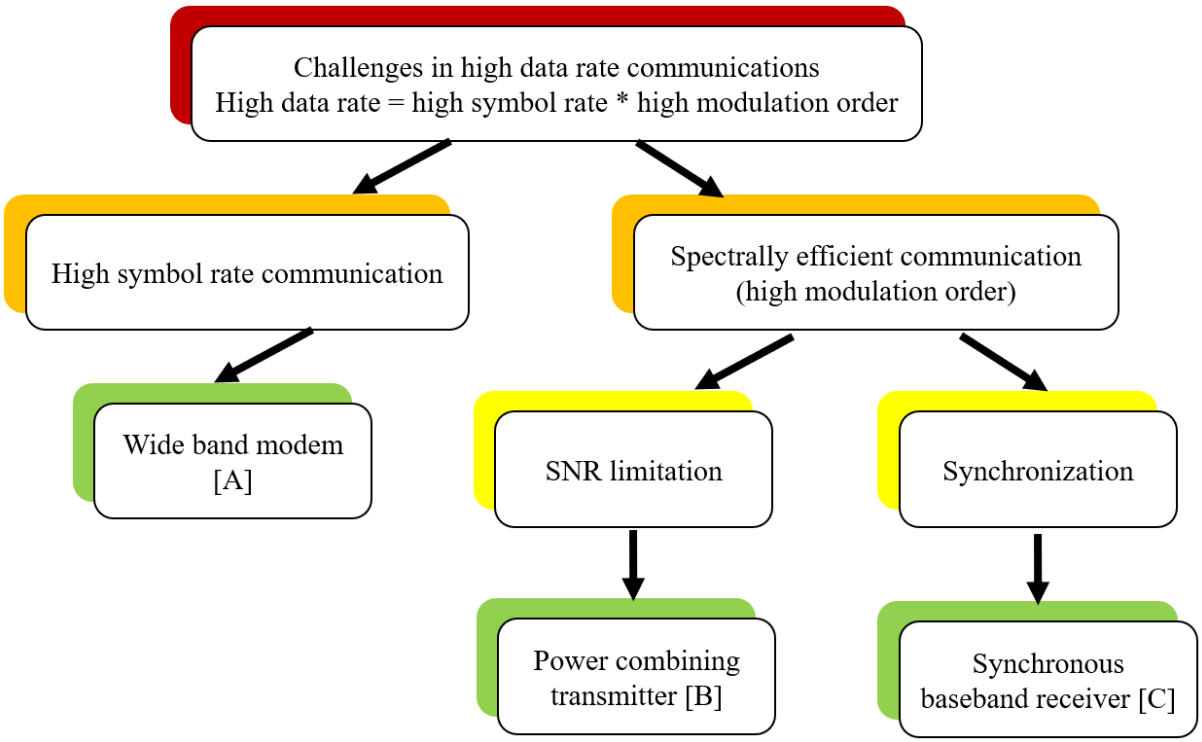

Fig. 1.6 Thesis outline in block diagrams.

Chapter 2

Multi-GHz Wideband Modem

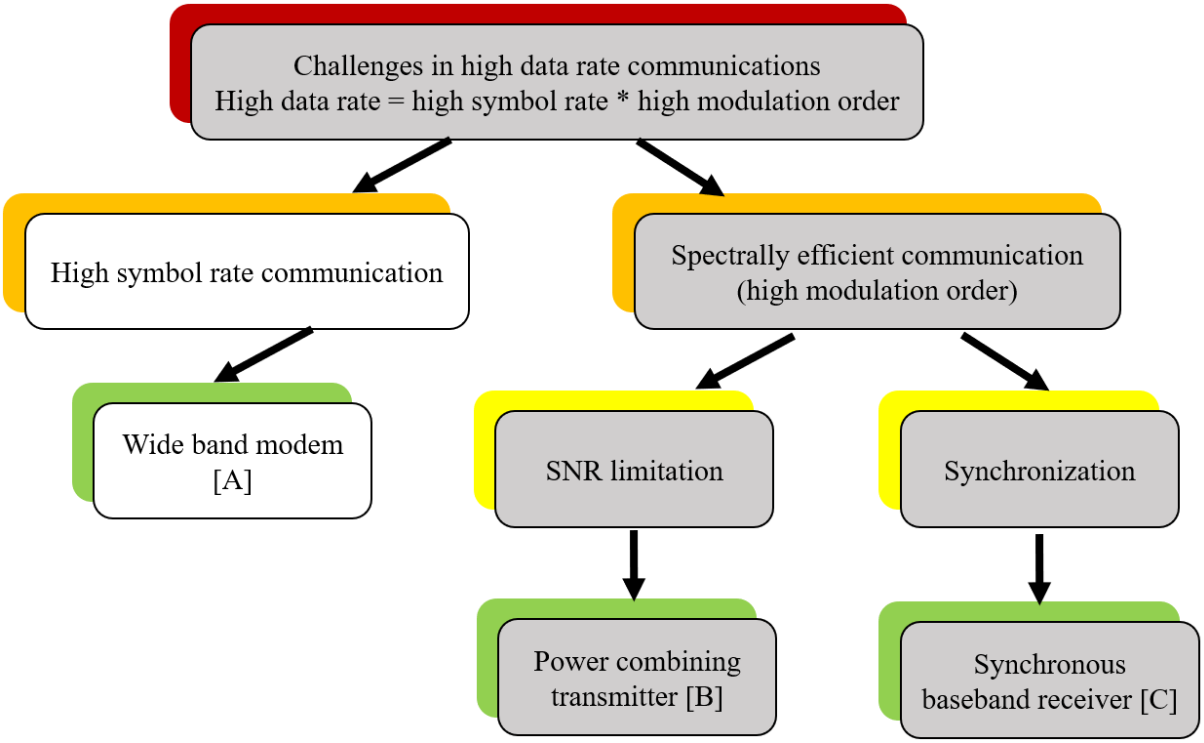

2.1 Differential phase shift keying

Differential phase shift keying (DPSK) is one of the most widely used modulation types which allows demodulation with non-coherent detection. Differential binary phase shift keying (DBPSK) can be implemented in a single channel transmitter and receiver while DQPSK needs a quadrature modem with I and Q channels. Compared with the on/off keying (OOK) and amplitude shift keying (ASK) modulation which also can be detected non-coherently, DQPSK has higher spectrum efficiency at the expenses of pre-coding at the transmitter side and corresponding decoder at the receiver side. Some experiments have been demonstrated regarding DPSK modulation and demodulation [37-39].

For phase shift keying (PSK) signals, the symbols are modulated on the phases using the carrier as a reference. At the receiver side, the carrier needs to be recovered to get the phase information. On the other hand, for DPSK signals, the symbols are modulated on the phases using the previous symbol's phase as a reference. Take DBPSK as an example, assuming the input data sequence is $\{a_n\}$, the output sequence of the differential encoding is $\{b_n\}$. Both of them are sequences with only two symbols 0 and 1. The differential encoding is implemented as the Eq. 2.1 shows, where $\oplus$ is exclusive-OR (XOR). The encoding rule is also illustrated in the table.

$$b_n = a_n \oplus b_{n-1},\ a_n, b_n \in \{0,1\} \tag{2.1}$$

Table 2.1 DBPSK encoding rule

a_n	b_n	$\Delta\theta$
0	b_{n-1}	0
1	$\overline{b_{n-1}}$	180°

For DQPSK signals, the encoding rule is similar to that of DBPSK signals. In a QPSK signal, there are four possible phase differences to carry two information bits. The phase of a DQPSK modulated signal output is not only related to input binary bits but also related to the phase of the previously transmitted signal. Table 2.2 shows the encoding rule. Where x(k) is the input data sequence with four different symbols {00,01,10,11}. I(k) and Q(k) are the output symbol for I and Q channel, $\Delta\theta$ is the phase difference between two adjacent symbols. At the receiver side, the received signal still have four different phases as QPSK signal. While the transmitted symbol can be recovered by comparing the carrier phase of two adjacent symbol periods.

Table 2.2 DQPSK encoding rule

X(k)	I(k)	Q(k)	$\Delta\theta$
00	$\overline{I(k-1)}$	$\overline{Q(k-1)}$	π
01	$Q(k-1)$	$I(k-1)$	$\pi/2$
10	$Q(k-1)$	$\overline{I(k-1)}$	$-\pi/2$
11	$I(k-1)$	$Q(k-1)$	0

2.2 Wideband DQPSK modem demonstrators

The D-band transceiver chipset with a 3-dB bandwidth of 40 GHz has been published in [1]. This gives a great opportunity for high data rate communication with a speed of tens of Gbps. Data transmission of a 48 Gbps QPSK signal has been verified on this D-band transceiver chipsets in a shared LO (fully synchronized) configuration [24]. Advanced equipments are used to provide a baseband signal and to demodulate the signal. In addition to wide-band mm-wave transceivers design, another challenge in realizing ultra-high capacity radio systems is to implement wide-band modulators and demodulators (modems) that can work in real-time. As shown in Fig. 2.1, differential encoder and wideband demodulator hardware are added to the transmitter and receiver chipset to form a real-time D-band communication link. In the transmitter side, the differential encoder is realized in an FPGA which generates I and Q baseband signals from a pair of input binary data streams. A D-band transmitter chipset is used to up-convert the baseband signal to a radio frequency signal and amplify the signal afterward. At the receiver side, the received signal is amplified and then down-converted to an IF stage by a D-band receiver chipset. After that is a DQPSK demodulator which performs differential detection to recover the transmitted data by using analog components.

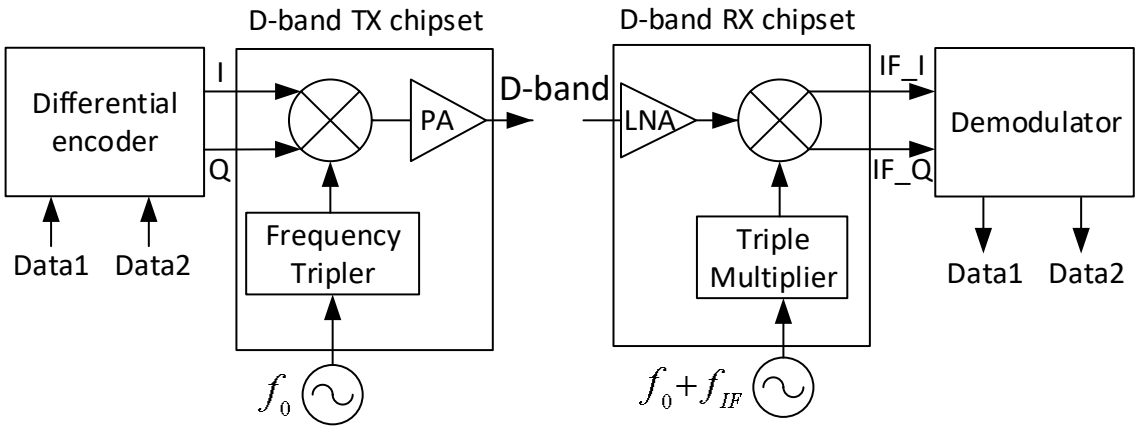

Fig. 2.1 The system structure of the D-band communication link.

The differential encoding is implemented on a single FPGA which provides four transceiver channels with data rate up to 28 Gbps for each channel. The structure of differential encoder is shown in Fig. 2.2. The differential encoder takes dual 20 Gbps data input streams and encoded these streams into 20 Gbaud DQPSK baseband I and Q signals. The detail encoding process has been explained in [38]. The outputs from the FPGA are modulated up to a D-band carrier using a D-band transmitter (TX) so that a 40 Gbps DQPSK signal is generated. Two options are provided as the data input: internal pseudo-random binary sequence (PRBS) generator in the FPGA and data from external sources. The input data has to be de-serialized (DeMUX) and interleaved before performing differential encoding because of the clock frequency limitation of the FPGA. After de-interleaving and serializing (MUX), encoded baseband signals are provided to the D-band TX chipset.

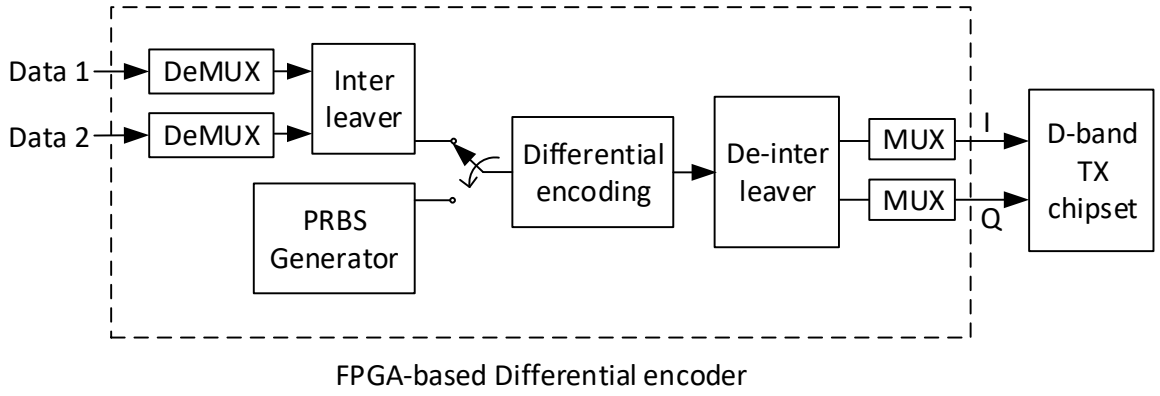

Fig. 2.2 The architecture of the differential encoder.

As mentioned previously, the transmitted data can be recovered by comparing the phase of two adjacent symbols, which is called differential detection. After the received signal is converted to an IF, a delay line and a phase detector are needed for detection. The implementation of the proposed DQPSK demodulator is illustrated in Fig. 2.3. The phase detector is realized by an XOR and a low pass filter (LPF). The received signal is down-converted by the D-band chipset to IF stage. The RX chipset provides differential I and Q output. Only one delay element is needed which provide a time delay of one symbol period plus a 45-degree phase shift at the IF frequency. Then the delayed IF_Q- is mixed with IF_I+ and IF_Q+.

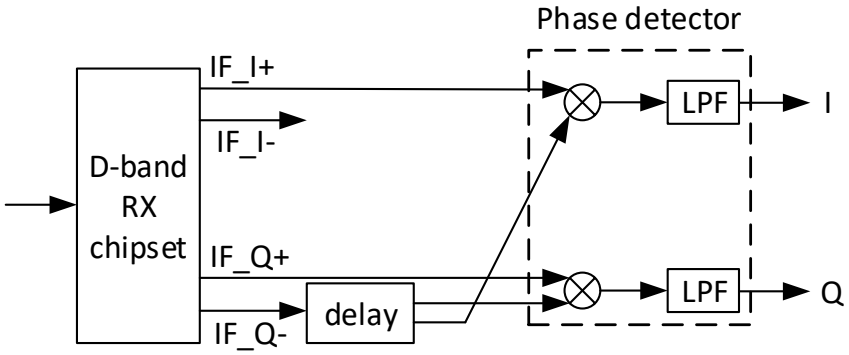

Fig. 2.3 The architecture of the DQPSK demodulator.

When the received signal is mixed with its delayed copy, the mixer output can be written as

$$\cos(\omega_{IF}t + \theta_1) \times \cos(\omega_{IF}t + \theta_2 + 45°)$$
$$= \frac{1}{2} \times [\cos(2\omega_{IF}t + \theta_1 + \theta_2) + \cos(\theta_1 - \theta_2 - 45°)]. \quad (2.2)$$

After it passes the LPF, the first part in Eq. 2.2 will be filtered out, the output becomes

$$V_{out} = \frac{1}{2} \times \cos(\theta_1 - \theta_2 - 45°) = \frac{1}{2}\cos(\Delta\theta - 45°)\,. \quad (2.3)$$

The phase detector output can be expressed as

$$\Delta\theta = \arccos(2 \times V_{out}),\ 2V_{out} \in [-1, +1] \quad (2.4)$$

For DQPSK, $\Delta\theta = 0, \pi/2, \pi, 3\pi/2$, the output V_{out} corresponding to 1/2, 1/2, -1/2, -1/2. So that phase 0 and $\pi/2$ cannot be distinguished, phase π and $3\pi/2$ cannot be distinguished.

Fig. 2.4 shows the relationship between $\Delta\theta$ and V_{out}. The detection range for this phase detector is from 0 to π. So, for DQPSK signal, both I and Q channel are needed to detect all four phases. By having an additional information of

$$V_{out,Q} = \frac{1}{2} sin(\Delta\theta - 45°) \, . \tag{2.5}$$

The $\Delta\theta$ can be recovered with no ambiguity.

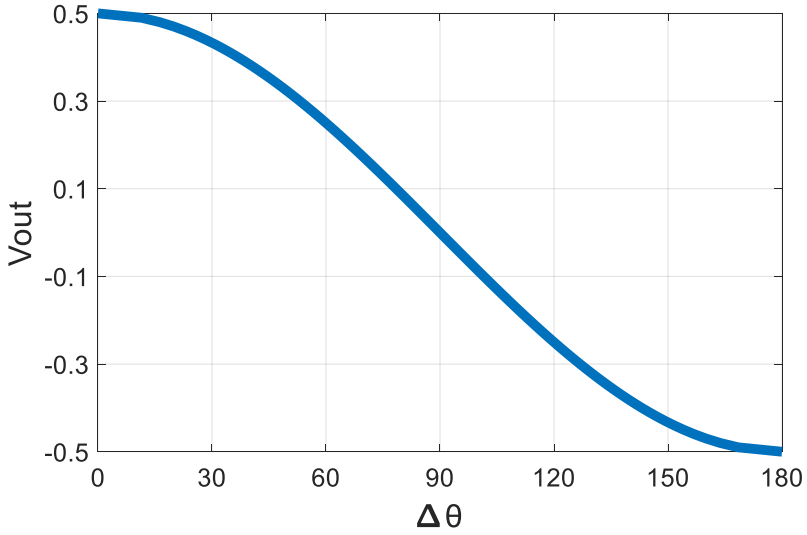

Fig. 2.4 Detection range of the phase detector.

2.3 Performance verification

2.3.1 Differential encoder test

The FPGA based differential encoder is tested with the internal PRBS generator and the output signals from I/Q channel are received by the oscilloscope to observe the eye diagram. The captured eye diagram of I channel is shown in Fig. 2.5. The symbol rate is 20 Gbaud. For QPSK signal, it could provide baseband QPSK signal with a data rate of 40 Gbps.

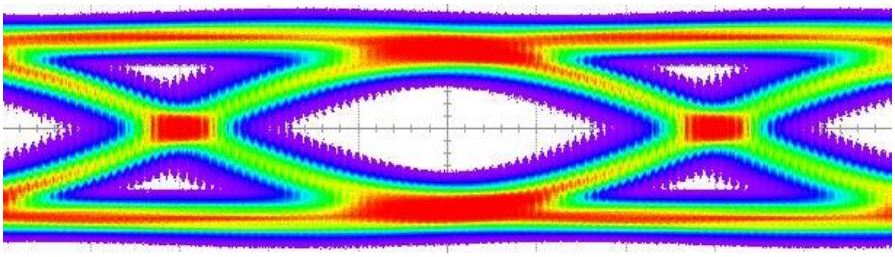

Fig. 2.5 Eye diagram of the 20 Gbaud signal from FPGA.

2.3.2 Demodulator test

The measurement setup structure for verifying the performance of the demodulator is shown in Fig. 2.6. An arbitrary waveform generator is used to provide two channels of 20 Gbps DQPSK signal modulated on a 10 GHz carrier. These two channels have a 90-degree phase shift so that they can be regarded as I and Q channel. The signal in the Q channel is further divided into two branches. The lower branch signal with a tunable delay provides the signal with one symbol

period delayed and 45-degree phase shift, which mixes with both I and Q signal to realize the differential detection. The XOR (HITTITE HMC844LC4B) is used together with LPF as a phase detector. Finally, an oscilloscope (Teledyne Lecroy LabMaster 10-100Zi) is connected with the output of the demodulator to observe the recovered signal. The eye diagrams of recovered I and Q signal are shown in Fig. 2.7. The estimated bit error rate from the eye diagram is 10^{-24}.

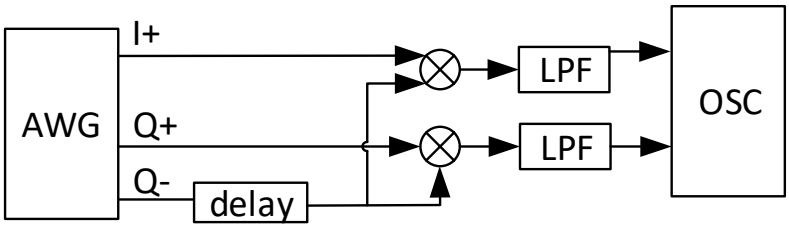

Fig. 2.6 Test structure of the demodulator.

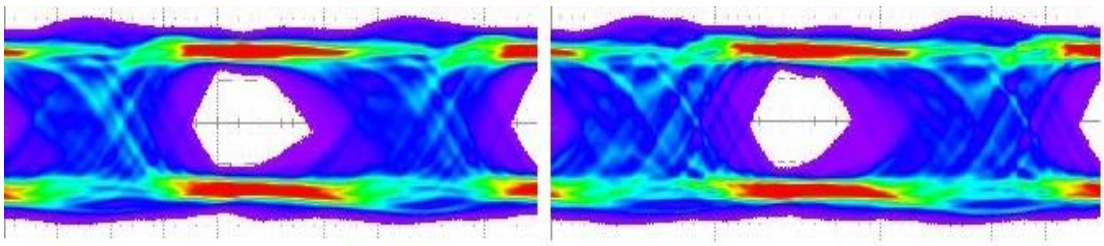

Fig. 2.7 Eye diagram of the recovered I/Q data as shown in the oscilloscope.

As discussed previously, the tunable delay element should provide one symbol period delay and 45-degree phase shift at IF frequency. For example, for a 10 Gbps DBPSK signal on a 20 GHz carrier, the delay should provide a time delay of

$$\frac{1}{20\times10^9}\times\frac{45}{360}+\frac{1}{10\times10^9}=1.0625\times10^{-10}\ \text{s}. \tag{2.6}$$

To ensure that the delay element provides the desired time delay, a test setup for delay adjustment has been made. The structure of the setup is shown in Fig. 2.8. The pulse pattern generator (PPG) is used to provide a pulse pattern with a thousand continuous '0' and one '1'. This single pulse signal splits into two branches, the lower branch signal passing through a delay element and then mixed with the upper branch signal by an XOR. The output signal of the XOR goes into the oscilloscope. There are two pulses shown in the oscilloscope, the time delay between them can be measured by an oscilloscope. Therefore, the delay elements can be tuned to provide the exact desired time delay.

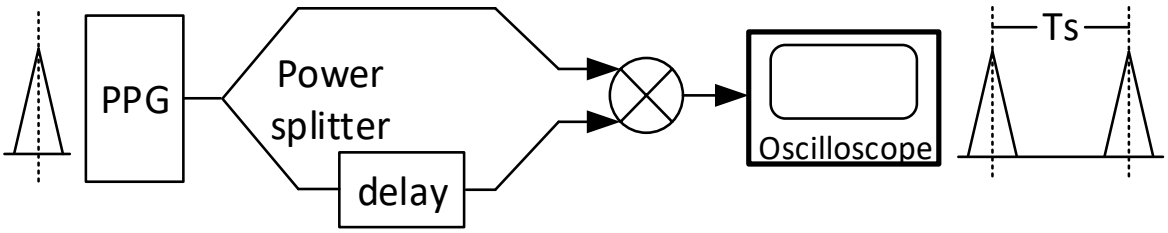

Fig. 2.8 Set-up for the delay adjustment.

2.3.3 **Modem capacity test**

The AWG could provide only 20 Gbps DQPSK at 10 GHz IF carrier for demodulator verification due to its bandwidth limit. Whereas the FPGA based modulator could provide 40 Gbps DQPSK signal. To further verify that the modem's capability, the demodulator is tested with 20 Gbps signal in a single channel configuration. A measurement setup for this verification is shown in Fig. 2.9. A PPG is used to generate a 20 Gbps differential encoded baseband. The baseband signal is then modulated on a 20 GHz carrier by an XOR as a mixer. Next, an attenuator is followed to adjust the input power of the demodulator. After the demodulator, the detected signal is fed back to the bit error rate tester (BERT) for BER measurement and send into the oscilloscope for eye diagram observation.

The eye diagram of the recovered signal of 20 Gbps and 22 Gbps are shown in Fig. 2.10. The measured BER is 10^{-14} and 10^{-8}, respectively. The bandwidth of the XOR and the tunable delay limit the performance of this modem.

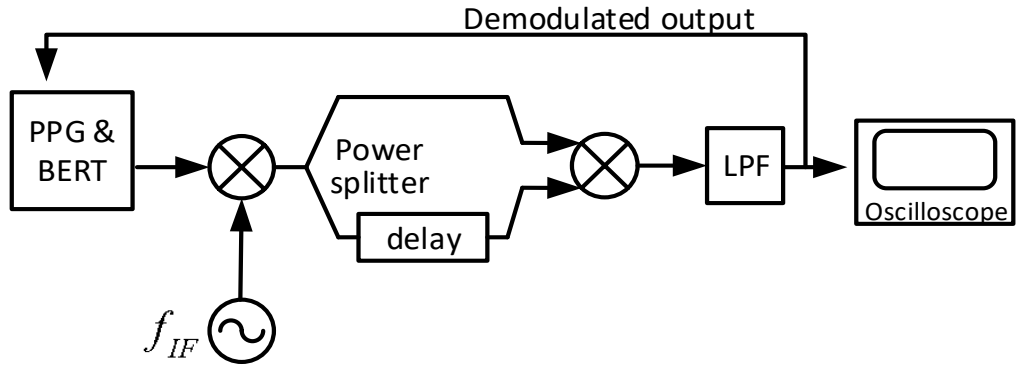

Fig. 2.9 Set-up for modem capacity test.

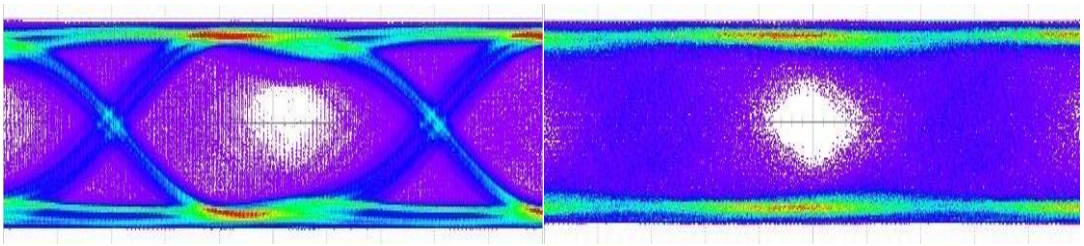

(a) (b)

Fig. 2.10 Eye diagrams as shown in the oscilloscope, (a) recovered data at 20 Gbps and (b) recovered data at 22 Gbps.

The input power, that the demodulator is needed for correct detection, is also studied. The measurement setup is shown in Fig. 2.11. An attenuator is added before the demodulator to adjust the input power. The input power and the demodulated signal's BER is estimated by the oscilloscope. Fig. 2.12 shows the input power range of the demodulator to achieve a BER smaller than 10^{-8} for different symbol rate. As the symbol rate increasing, the input power range for correct detection of the demodulator decreases. To achieve the same SNR, a high symbol rate signal needs more power. As a result, the minimum needed power of the demodulator increases as the symbol rate increase. The key component in the demodulator is the XOR (HITTITE HMC844LC4B). Its input power should be between -16 dBm to -6.5 dBm to make it work properly according to its datasheet. When the input power is outside this region, the

signal is distorted so that the BER increases. The high symbol rate signal is more vulnerable to this distortion so that the maximum tolerable power decreases as the symbol rate increases.

With the same setup, the IF frequency is tuned to learn the frequency range for correct detection. When the symbol rate is 10 Gbaud, 20 Gbaud and 22 Gbaud, the IF frequency is first set at10 GHz, 20 GHz and 22 GHz, respectively. Then the signal generator will adjust the IF frequency to achieve a BER smaller than 10^{-8}. The IF frequency range for different symbol rate is shown in Fig. 2.13. As the symbol rate increasing, the IF frequency range for correct detection of the demodulator decreases. The reason for that is the high symbol rate signal is more sensitive to the phase mismatch due to its short wavelength. A picture of the lab test-bed is shown in Fig. 2.14.

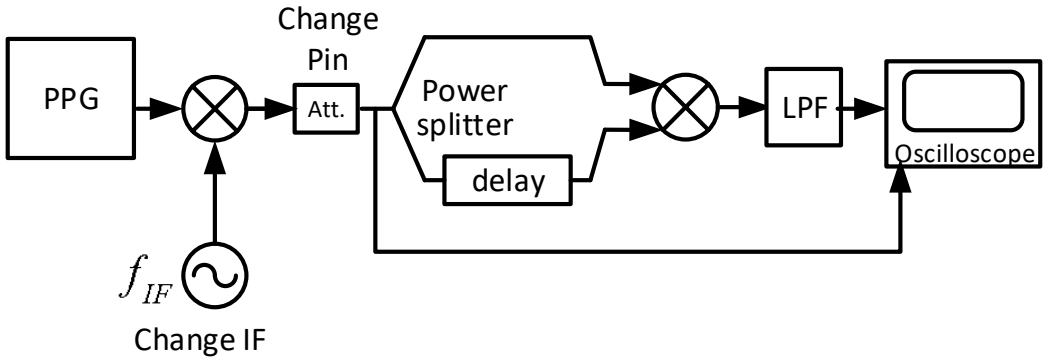

Fig. 2.11 Setup for demodulator input power test

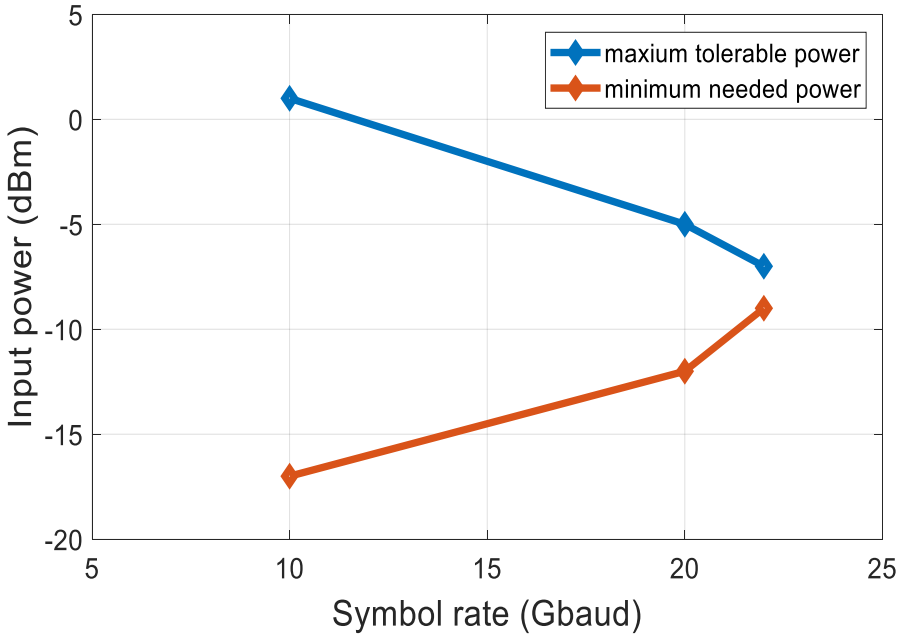

Fig. 2.12 Input power range of the demodulator

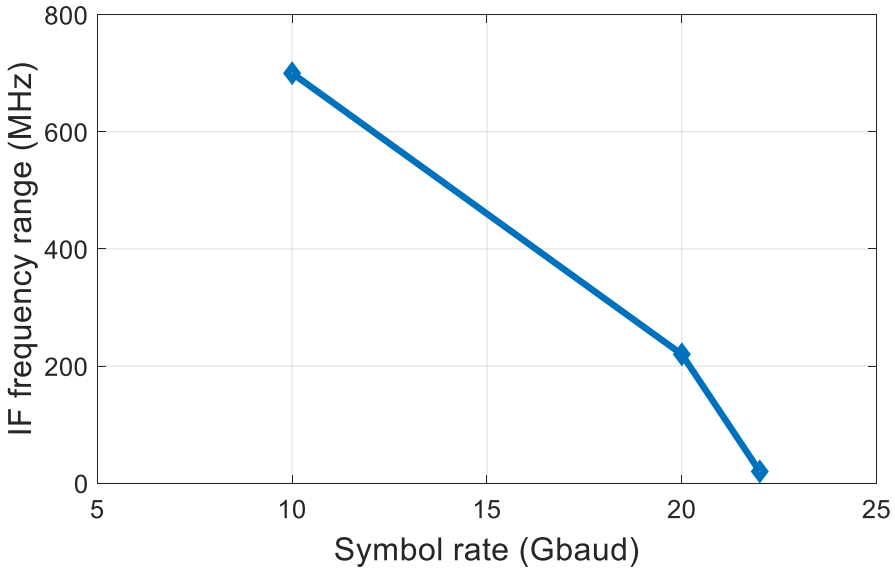

Fig. 2.13 IF frequency range of the demodulator

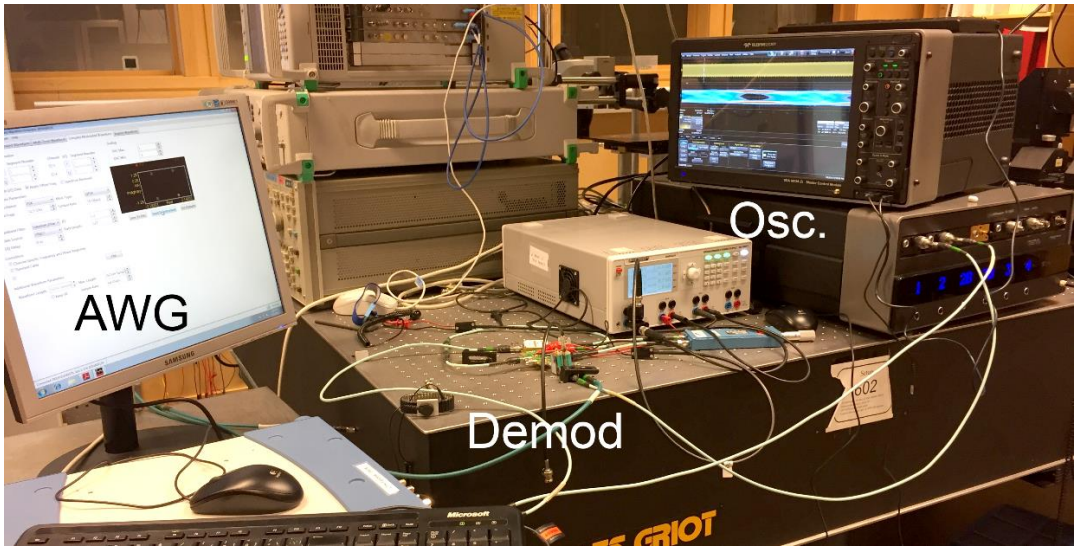

Fig. 2.14 Photo of the lab test-bed.

Chapter 3

Spectrally Efficient Communication: Power Combining Transmitter

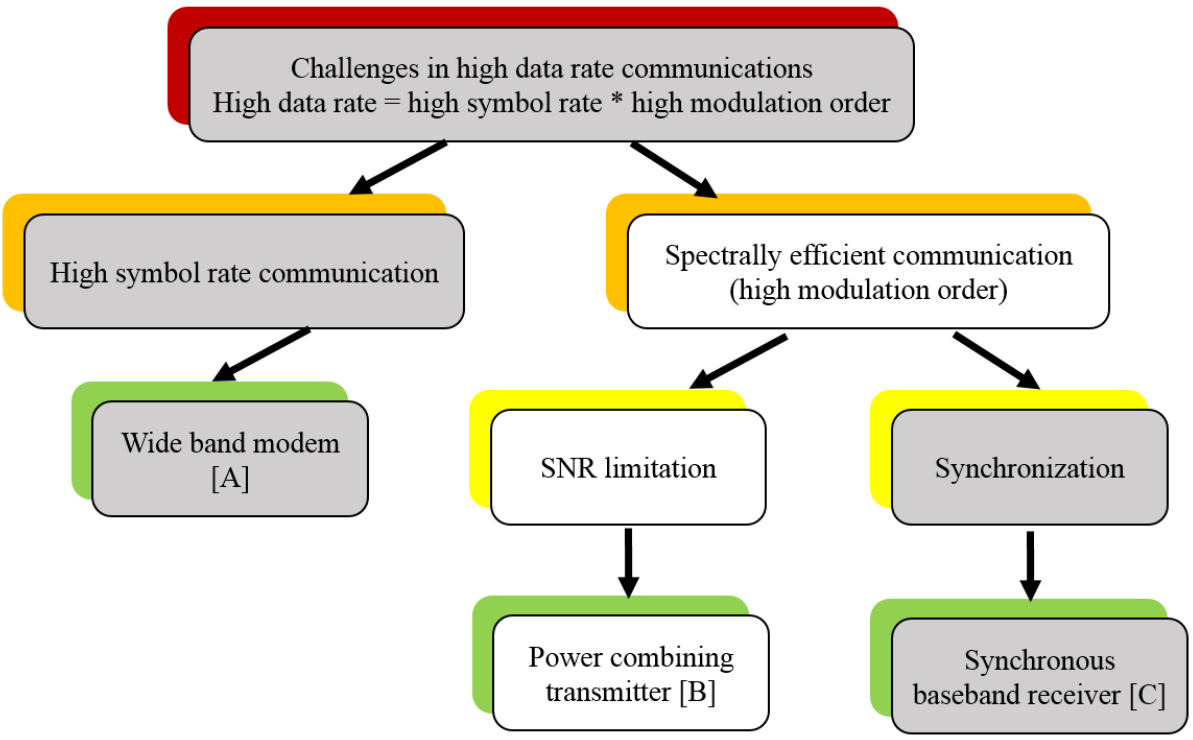

3.1 High-frequency power amplifier and non-linear distortion

As discussed in the previous chapter, millimeter-wave frequency bands provide a great opportunity for realizing high data rate communication. However, the output power of millimeter-wave power amplifiers (PA) is limited. Fig. 3.1 shows the saturation output power of a PA at W-band and D-band in recent years publications [40-51]. The output power that a D-band PA could provide is nearly 15 dB lower than a W-band PA, which limits the SNR of the transmitted signal. The SNR limit the modulation order as well as spectrum efficiency.

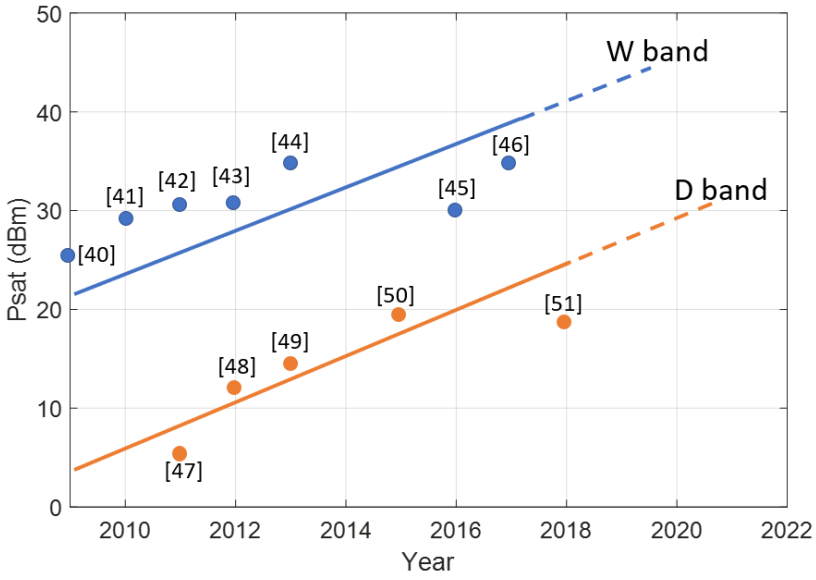

Fig. 3.1 Saturation output power of a PA at W-band and D-band

Fig. 3.2 shows a general relationship between the input power and the output power of a power amplifier. As the input power increases, the output power first increases linearly. Increasing the input power further, the amplifier starts working in its non-linear region and the output power increases slower. When the input power keeps adding until the amplifier works in its saturation region, the output power remains constant at its saturating level. In most cases, the saturated output power that an amplifier could provide cannot be used, because it will cause non-linear distortion to the signal after amplification.

To avoid the non-linear distortion, the input power needs to back-off several dB to ensure the amplifier works in its linear region. This operation will further decrease the SNR. In order to increase the SNR and use a high order modulation signal in the communication system, the power back-off need to be avoided.

A solution to this problem is using digital pre-distortion (DPD). The main idea of DPD is to compensate the non-linear effect prior the signal goes into power amplifiers. All these DPD solutions use feedback loops to realize the compensation, which means it is difficult to implement wideband compensation in real time. DACs and ADCs are key components in this loop. Because of the sample rate limitation of DACs and ADCs, the data rate of the

communication system is limited. The communication data rate is around 10 to 100 Mbps while using DPD techniques [52-53]. The outphasing power combining technique is another solution to avoid the power back-off in PAs, which is explained in detail in section 3.3.

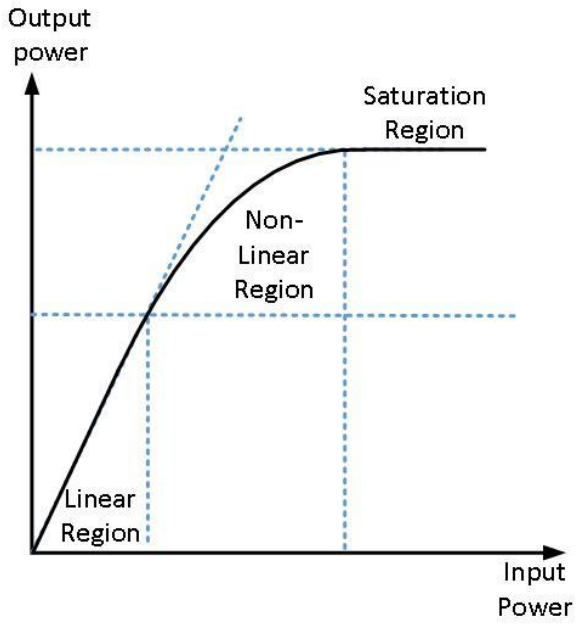

Fig. 3.2 Output power vs. input power curve of a power amplifier.

3.2 AM-AM distortion and AM-PM distortion

There are two kinds of distortion that amplifiers could bring, namely, amplitude to amplitude (AM-AM) distortion and amplitude to phase (AM-PM) distortion. This means the gain and the phase delay of the signal differ along with different input power level. Fig. 3.3 and Fig. 3.4 exhibit a typical amplifier gain and phase delay characteristics at different input power levels.

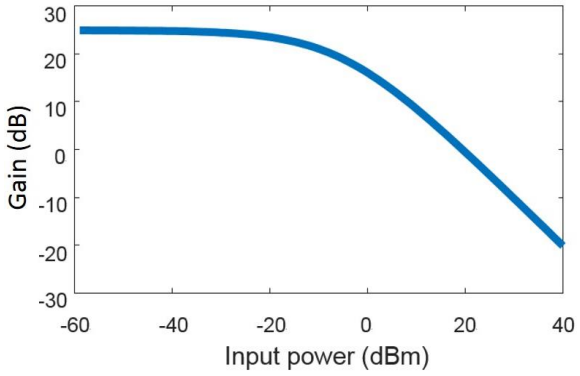

Fig. 3.3 Gain of an amplifier.

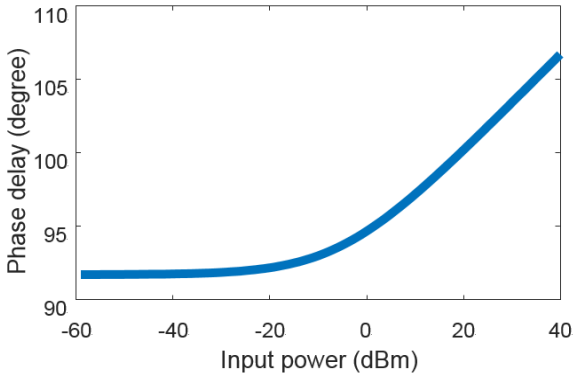

Fig. 3.4 Phase delay after amplification.

High modulation order signals with high PAPR would suffer more from the non-linear distortion. Take 16-QAM signals as an example, it has sixteen constellation points with three different amplitude levels. With the input power is backed-off, a distortion-free constellation can be observed after amplification, though with a power level less than the amplifier's

saturation level. With increasing the input level, the output constellation power increases, however, the constellation points will suffer from deformation as Fig. 3.5 shows. With different input power, the gain is different. The outer circle points with the least gain are compressed. In addition, the phase delay is also different with different input power. Outer circle points suffer from more phase rotation than the inner circle points do. So that the error vector magnitude (EVM) increases after the signal gets amplification.

However, for PSK signals, such as 8-PSK or 16-PSK, all constellation points have the same amplitude. With the same input power, all constellation points experience the same AM-AM distortion and AM-PM distortion. As a result, the shape of the constellation keeps the same.

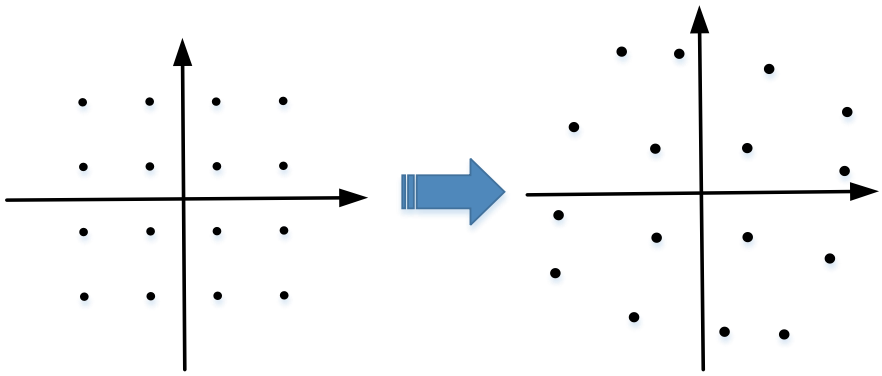

Fig. 3.5 Non-linear distortion of a 16-QAM signal after amplification.

3.3 Symbol-based outphasing technique

Even though power amplifiers have these non-linear effects on amplitude and phase, but with a fixed input power, the AM-AM and AM-PM distortion are fixed. So for signals which have a constant envelope, there will be no need to back off in output power. So if a signal can be generated by combining two signals of constant amplitude, then the AM-AM and AM-PM distortion can be ignored. Furthermore, the entire power range of amplifiers can be used. The outphasing technique is one way to achieve this goal.

The basic principle of outphasing is illustrated in Fig. 3.6. The transmitted signal can be represented as $S(t) = A(t)e^{j\theta(t)}$, where the transmitted information is modulated into amplitude $A(t)$ and phase $\theta(t)$ of the carrier. Signal $S(t)$ can be decomposed into two signals. By controlling the outphasing angle $\phi(t)$, the amplitude of decomposed signals can be set to any value in $(\frac{A(t)}{2}, \infty)$. So two signals can be choose as:

$$S_1(t) = \frac{A_{max}}{2} e^{j[\theta(t)+\phi(t)]} \tag{3.1a}$$

$$S_2(t) = \frac{A_{max}}{2} e^{j[\theta(t)-\phi(t)]} \tag{3.1b}$$

$$A_{max} = max\{A(t)\} \tag{3.1c}$$

where the amplitude of $S_1(t)$ and $S_2(t)$ is a constant value as half of the maximum amplitude of $S(t)$, $\phi(t)$ is the outphasing angle between decomposed signals and the original signal $S(t)$. And the outphasing angle $\phi(t)$ can be represent as:

$$\phi(t) = arccos(A(t)/A_{max}). \tag{3.1d}$$

With this decomposition technique, arbitrary waveform (i. e. QAM modulated signal) can be decomposed into two signals of constant envelope. When these two signals get amplified by two identical power amplifiers, the AM-AM and AM-PM distortions are identical. Combining two amplified signals together, an amplified original signal is generated without any non-linear distortion.

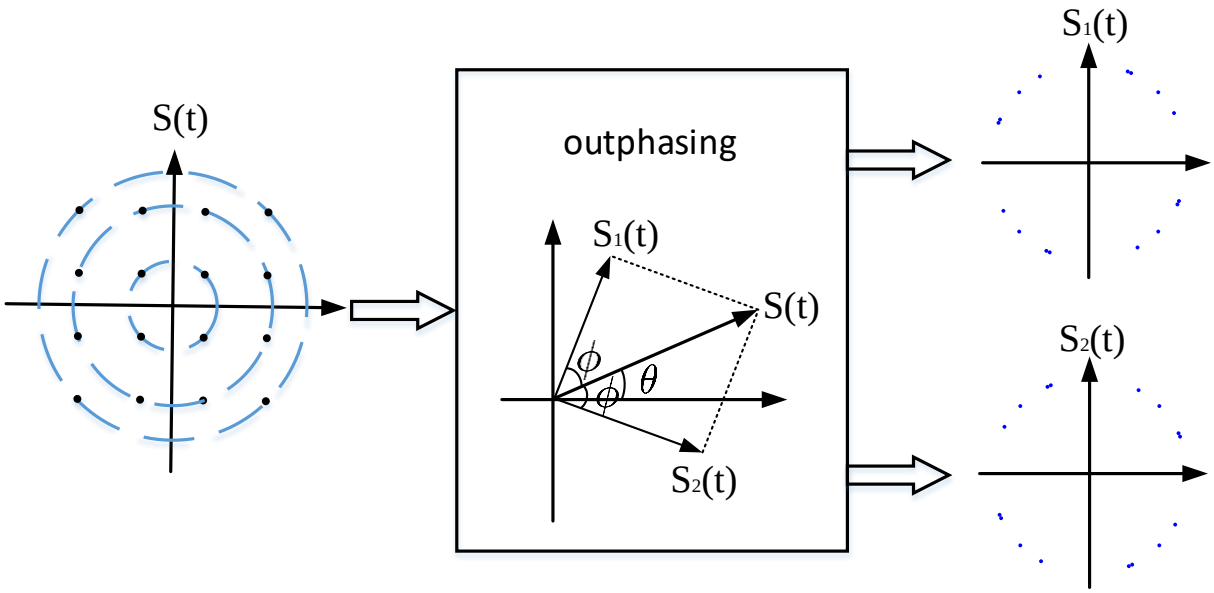

Fig. 3.6 Symbol-based outphasing technique.

The idea was first explored for achieving both linear operation and high efficiency. This technique, which originated in the 1930s, is referred to as "Linear Amplification with Nonlinear Components" or "Outphasing" [54-55]. It is traditionally implemented on the RF signal by analog circuits. In our case, we use digital signal processing to implement this outphasing technique to symbols, and then convert them to the analog baseband signal, mixed with LO signal and get amplified by analog devices.

However, the bandwidth limitation is not considered in most of the outphasing power combining systems. Taking the BPSK signal as an example, it has a constant envelope when the baseband signal is in the square wave shape. However, this results in unlimited bandwidth in the spectrum. In a real communication system, the baseband signal needs to pass a pulse shaping filter before modulating the RF signal. A pulse shaping filter, such as raised cosine filter, root raised cosine filter or Gaussian filter, limits the bandwidth of the baseband signal which also brings the fluctuation to the envelope. Outphasing technique splits the band-limited signal into two constant envelope signals with phase as the only modulated quantity. The

outphasing operation will introduce quick phase changes which widen the bandwidth. This is the reason for most of the outphasing power combining systems only demonstrate with low symbol rate below 200 Mbaud. A simulation of the spectrum of a baseband signal before and after outphasing is shown in Fig. 3.7. In this simulation, a 10 kbaud 16-QAM signal is used as an example.

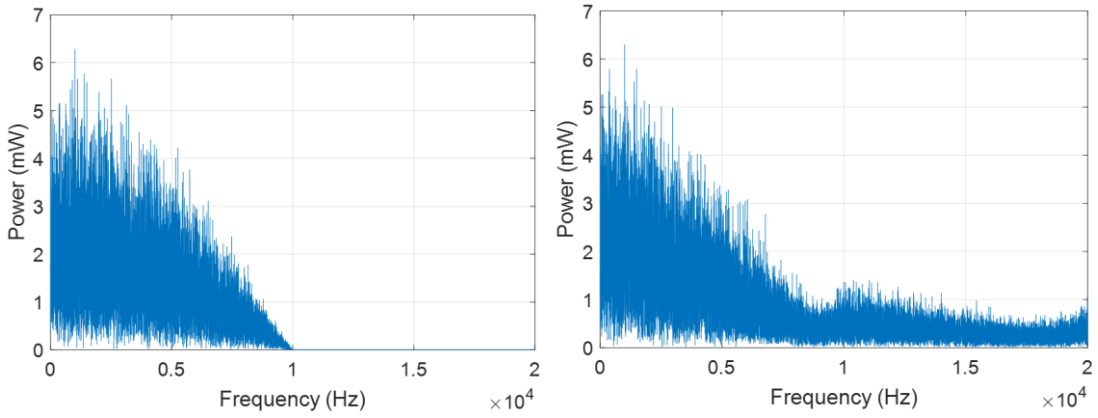

Fig. 3.7 The spectrum of the baseband signal before (left) and after (right) outphasing

The proposed symbol-based outphasing technique is to implement the outphasing operation to the symbols into two new symbols with the same amplitude but different phases. Two outphasing symbols can be represented as:

$$S_1[n] = \frac{A_{max}}{2} e^{j[\theta[n]+\phi[n]} \tag{3.2a}$$

$$S_2[n] = \frac{A_{max}}{2} e^{j[\theta[n]-\phi[n]}. \tag{3.2b}$$

They are pulse shaped before upconverted to RF, the modulated RF signal can be written as:

$$S_{RF1}(t) = \sum_{n=-\infty}^{+\infty} Re\{S_1[n] \cdot g(t - nT_s) \cdot e^{-j2\pi f_{RF} t}\} \tag{3.3a}$$

$$S_{RF2}(t) = \sum_{n=-\infty}^{+\infty} Re\{S_2[n] \cdot g(t - nT_s) \cdot e^{-j2\pi f_{RF} t}\}, \tag{3.3b}$$

where $g(t)$ is the pulse shaping filter response, f_{RF} is the carrier frequency and T_s is the symbol period. In this case, the bandwidth is defined but the envelope is no longer constant. However, at the optimal sampling points, the centre of a symbol period, the amplitude are same.

The purpose of power combining is to increase the SNR of the transmitted signal so that the communication data rate can be increased correspondingly. The traditional outphasing couldn't meet the requirement of high data rate communication. While the proposed symbol-based outphasing power combining technique is a solution to lower the signal's PAPR and keep the limited bandwidth at the same time.

3.4 System structure

The structure of the outphasing power combining transmitter is shown in Fig. 3.8. In this case, the baseband 16-QAM signal first use outphasing technique to decompose into two signals. Then these two signals both mixed with the RF carrier and send into power amplifiers. Finally, the amplified RF signals are combined together and sent out by an antenna.

Another power combining structure is showed in Fig. 3.9. Instead of using a power combiner and one antenna, the amplified RF signals are sent out by two antennae and combined in air. This structure gives a benefit of more output power by avoiding the insertion loss of the power combiner. The receiver can only receive the right message by having the right receiving angle where the path loss and delay from both antennae are identical. If two transmitted signals arrive in the receiver antenna with different phase and amplitude, then the transmitted message will not be able to recover. This structure can make the whole communication system more secure. At the transmitter side, a phase shifter could be added into the structure to adjust the desired receiving position. By using two antennae, the implementation complexity also increases.

In the work published in paper [B], only the structure shown in Fig. 3.8 is investigated.

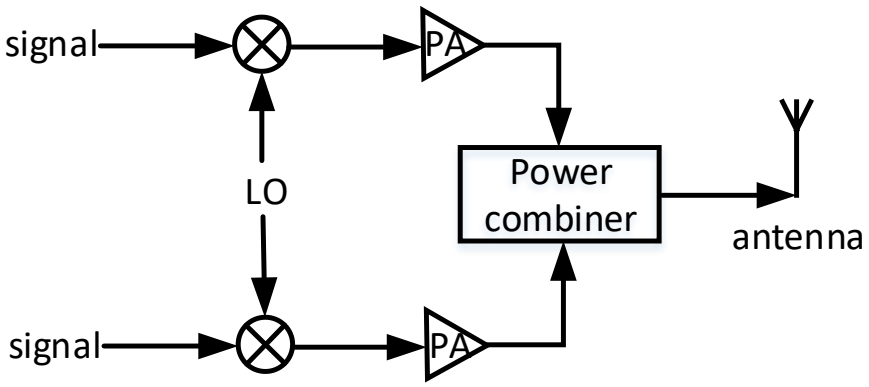

Fig. 3.8. Power combining structure with a combiner.

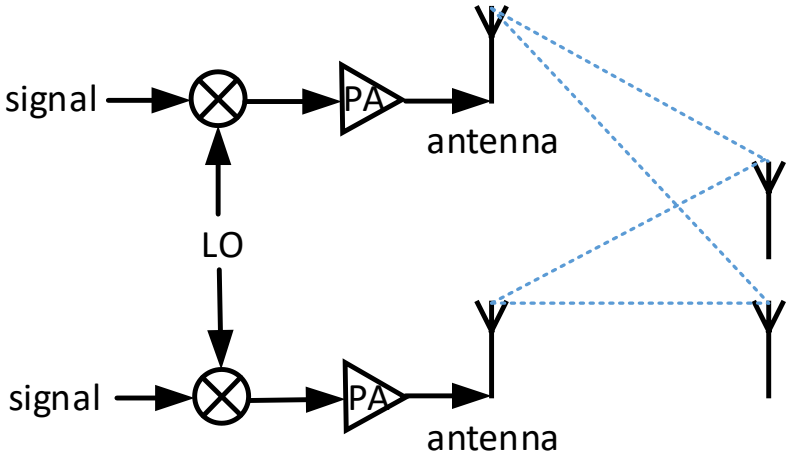

Fig. 3.9. Power combining structure with two antennae.

3.5 Performance verification

To verify the proposed outphasing transmitter topology, the transmitter is tested with continuous wave (CW) signal and modulated signal, respectively. The output power and EVM are observed in several conditions including the single transmitter, the dual transmitter of identical signal combining, dual transmitter outphasing combining.

3.5.1 CW test

First, a CW signal test is made to validate the transmitter's performance. The measurement setup structure is shown in Fig. 3.10. The CW signal was generated by an Arbitrary Waveform Generator (AWG), whose output power can be adjusted. After passing through an E-band transmitter module (SiversIMA FC1002E) and an attenuator, the signal was received by an oscilloscope. The received signal power was calculated by an oscilloscope. This transmitter module comprises a mixer, a times-six frequency multiplier and a power amplifier. The mixer and power amplifier both introduce non-linear effects to the signal. So in this case, the transmitter's performance is first studied.

The CW signal power response curve is shown in Fig. 3.11. When input power changes from -18 dBm to -7 dBm, the output power increases from 1 dBm to 10 dBm. During this region the system is linear. The 1 dB compression point (P_{1dB}) is observed at -7 dBm input power, where the distortion occurs. When the output power is beyond 12 dBm, the transmitter module goes into its saturation region

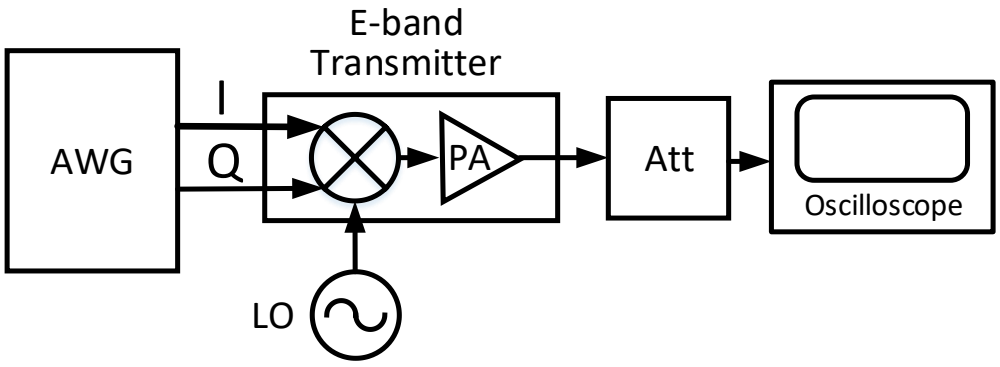

Fig. 3.10 Single tone test set-up.

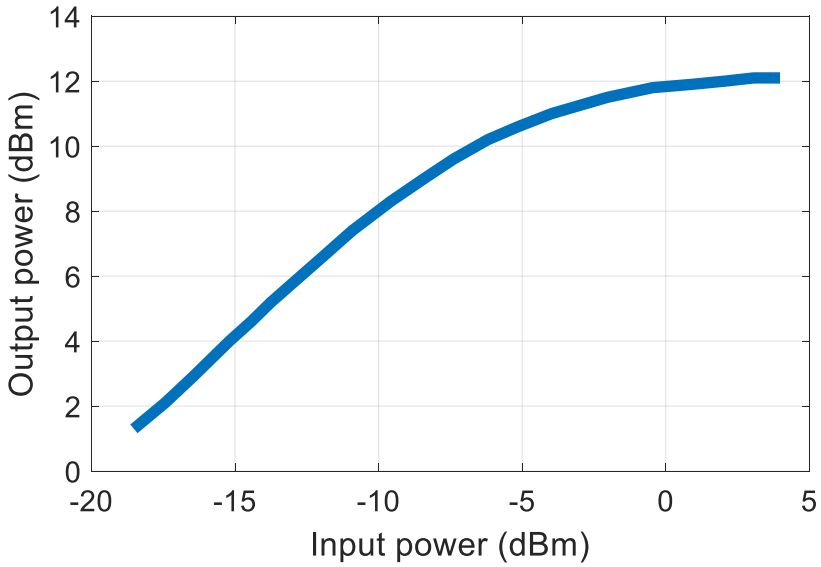

Fig. 3.11. CW signal power response.

3.5.2 **Modulated signal test**

To quantify the improvement in output power that the symbol-based outphasing technique could provide, measurements are performed with power combining two identical 16-QAM signals and power combining outphasing signals, respectively. The EVM and output power are measured in both cases.

The measurement setup is showed in Fig. 3.12. The symbol-based outphasing is implemented in Matlab. An AWG (Keysight M8195A, 8 bits, 65 GSps sampling rate) generates analog baseband I/Q signals as indicated in Eq. 3.2a and Eq. 3.2b. I_1 and Q_1 are from the complex signal $S_1(t)$. I_2 and Q_2 are from $S_2(t)$. After that, the baseband I/Q signals are sent into two E-band transmitters from SiversIMA. A signal generator is used to provide an LO signal. After amplification, two RF signals are combined together by a matched tee. A real-time oscilloscope (LeCroy LabMaster 10-100Zi, 100 GHz bandwidth, 240 GSps sampling rate) is used as a receiver. The Vector Signal Analysis (VSA) is used to demodulate the received RF signal and estimate EVM and BER through its constellation. An attenuator is inserted between the matched tee and the oscilloscope to avoid saturating the oscilloscope.

First, a single 16-QAM signal transmission with a single transmitter is tested to serve as a reference. Then two identical 16-QAM signals (I_1=I_2, Q_1=Q_2) are combined in-phase with two transmitters. Finally, the proposed symbol-based outphasing power combining is tested with the same setup. The carrier frequency is set in the middle of the passband (81 GHz to 86 GHz) of E-band transmitters at 83.5 GHz. A root-raise-cosine filter is used for pulse shaping function. The input power is controlled by the AWG. The measurement result is shown in Fig. 3.13, which illustrates the received signal's EVM versus the output power from the transmitter side. Fig. 3.14 shows the received signal's constellation diagram of combining two identical 16-QAM signals and combining outphasing signals with the same output power at the transmitter side of 10.7 dBm.

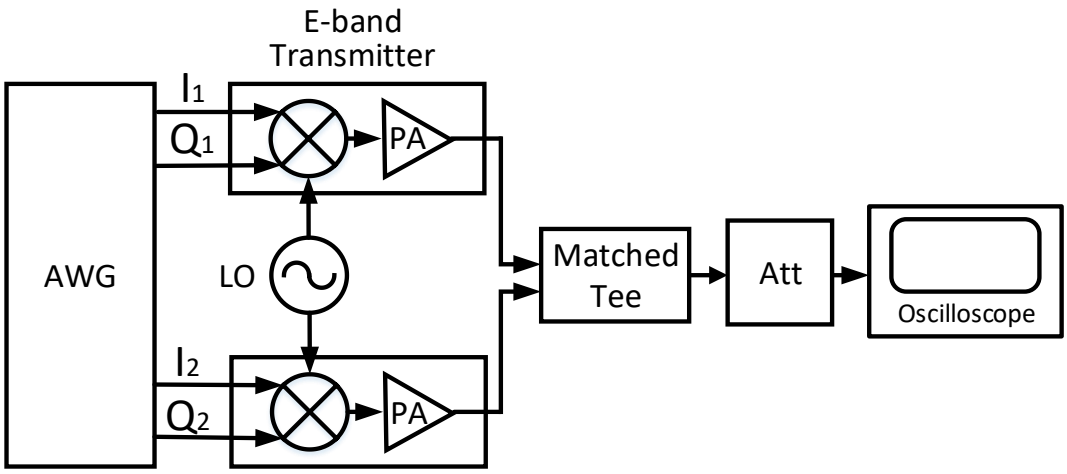

Fig. 3.12 Power combining system measurement set-up.

Using this power combining system, a 2 Gbaud 16-QAM signal has been tested. For single 16-QAM signal transmission measurement (red line), with the output power increasing at the transmitter side, the EVM increase rapidly when its output power is higher than 10 dBm. Combining two identical 16-QAM signal (yellow line) gives 1.5 dB more output power than the single transmitter case with the same EVM. In both cases, the EVM deteriorate as the output power increase due to the non-linear distortion. The constellation diagram is shown in Fig. 3.14(a) with an output power of 10.7 dBm and 13.19% EVM. The outer circle points are heavily distorted. Both AM-AM distortion and AM-PM distortion are observed in the received signal.

For symbol-based outphasing power combined signal (blue line), the EVM does not increase as fast as the other two cases. With the EVM below 12% (BER lower than 10^{-4}), the output power can reach 12 dBm. Comparing with other two curves with the same EVM of 12%, the signal using symbol-based power combining technique has 3 dB more output power than the single 16-QAM signal and 2 dB more power than the double 16-QAM combined case. And the constellation diagram in Fig. 3.14 (b) has a better shape than the double 16-QAM combined signal as well as a lower EVM of 10.87%. With a given output power beyond 9 dBm at the transmitter side, it provides better signal quality with lower EVM when amplifiers work in their non-linear region.

In summary, the symbol-based outphasing power combining technique could help to maintain the linearity of the signal after amplification. As a result, the transmitted signal could provide higher output power while keeping a low EVM. Compared with the other published transmitter using outphasing power combining technique summarized in Table 3.1, this work demonstrated the outphasing with the highest data rate at the highest carrier frequency.

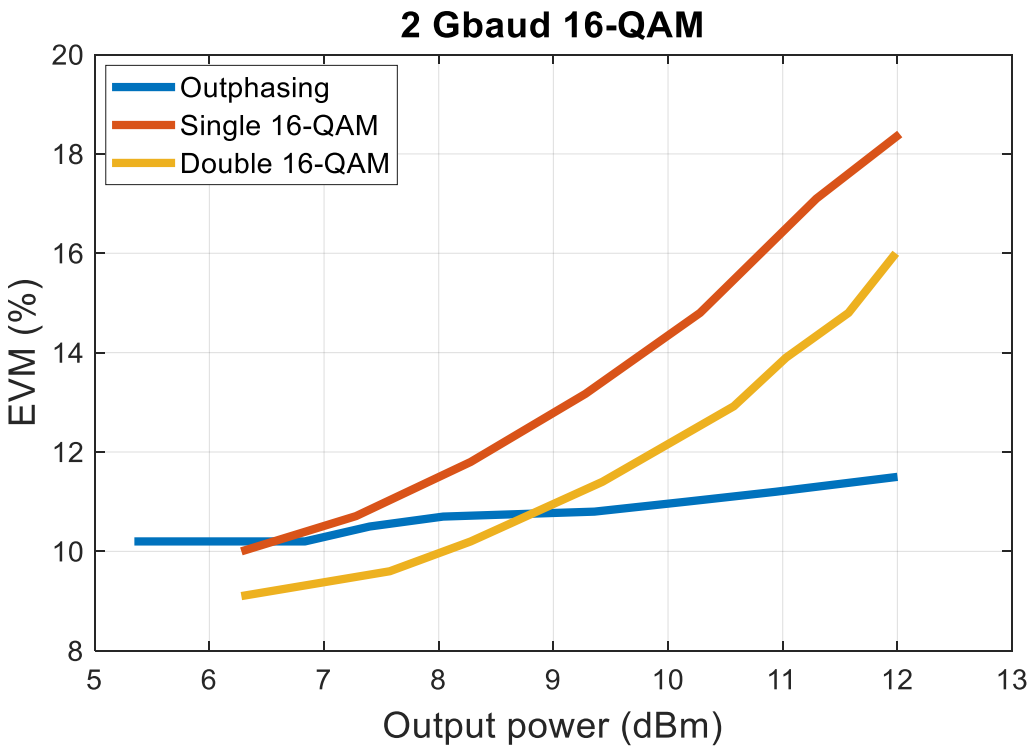

Fig. 3.13. Performance comparison of outphasing combining with conventional power combining and a single transmitter.

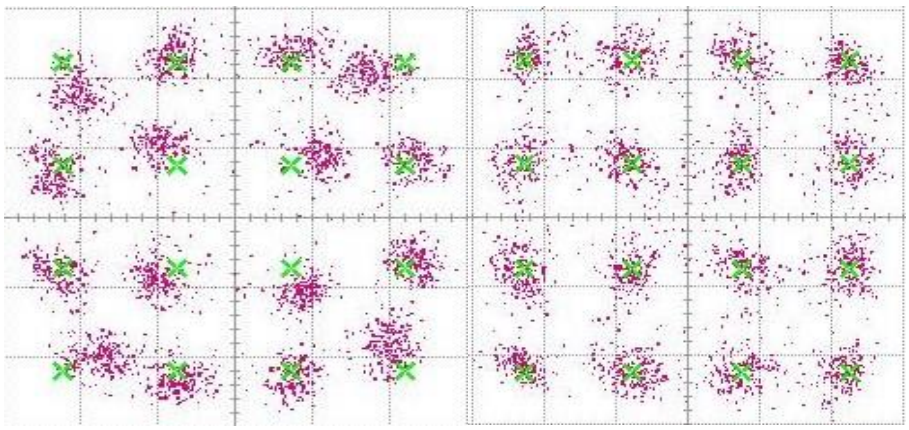

(a) double 16-QAM EVM=13.19%

(b) Outphasing EVM=10.87%

Fig. 3.14 Constellation of combined 16-QAM signal with 10.7 dBm output power

Table 3.1 Summary of published outphasing transmitters

Ref.	RF freq. (GHz)	Data rate (bps)	Baud rate (Baud)	Modulation	Power (dBm)
[56]	8	80 M	10 M	64-QAM	9.2
[57]	9.8	156 M	78 M	$\pi/4$ DQPSK	-1
[58]	10	1.1 G	80 M	256-QAM	23
[59]	60	200 M	50 M	16-QAM	9.7
[60]	60	500 M	125 M	16-QAM	12.5
This work	**83.5**	**8 G**	**2 G**	**16-QAM**	**12**

Chapter 4

Spectrally Efficient Communication: Synchronous Baseband Receiver

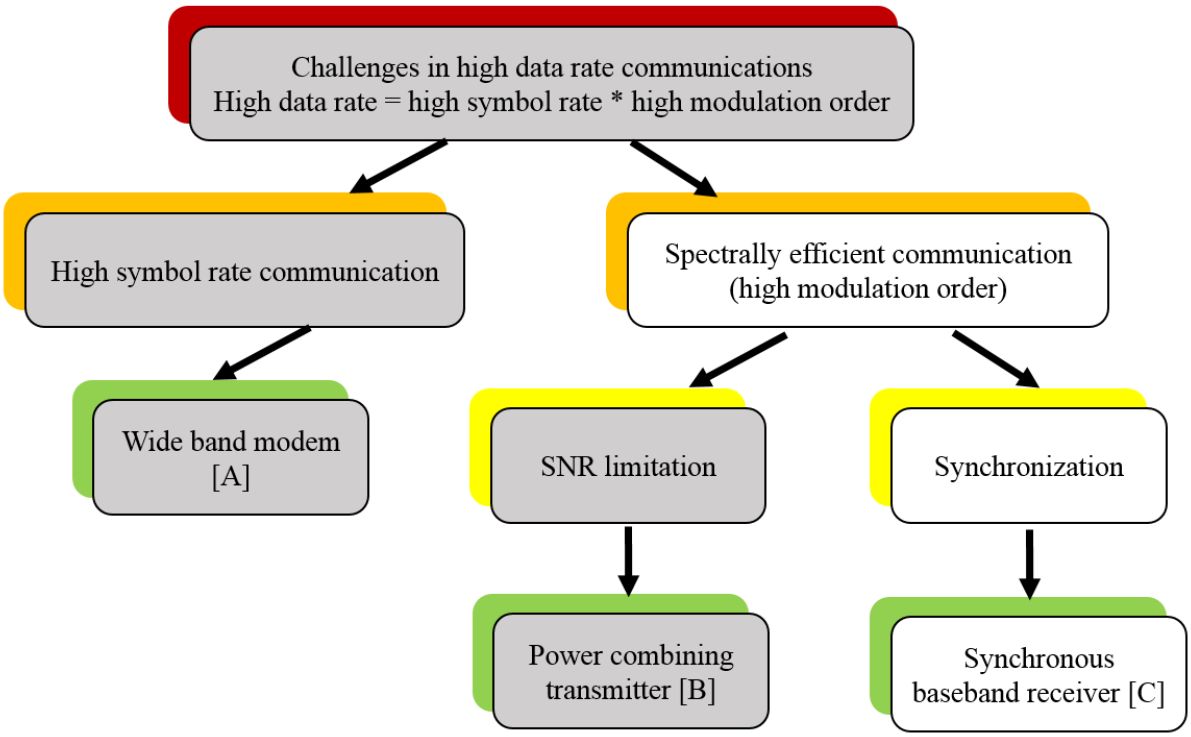

4.1 Overview of published millimeter-wave transmissions

Communications in millimeter-wave frequencies have been demonstrated in recent publications. It can be sorted into two groups: with or without real-time demodulation. With the help of advanced laboratory equipment and off-line DSP, the non-real-time transmission has been demonstrated at very high data rate up to 100 Gbps [32]. These results indicate the millimeter-wave frequency front-end transceiver chipsets already have capabilities to support high data rate transmissions.

Table 4.1 summarizes some published real-time transmission experiments over millimeter-wave bands. Real-time transmissions are demonstrated with either high data rate few bits per symbol or low data rate many bits per symbol. The maximum data rate in real-time millimeter-wave transmissions at the moment is 42 Gbps using a 2-ASK signal [23]. The highest modulation order has been successfully transmitted in real-time is 64-QAM, with a single-channel data rate of 5.3 Gbps [33].

For low modulation order signals, such as OOK, ASK, BPSK or QPSK, real-time demodulation can be realized by non-coherent detections. Such as OOK and ASK signals, by detecting the amplitude of the received signals, the transmitted data can be recovered. For BPSK and QPSK signals, as illustrated in Chapter 2, differential coding and detection could help in realizing real-time demodulation. For PSK signals, there are two well-known methods to implement demodulation, Costas loop [20] and multiplication [61]. However, the structure of the Costas loop becomes more complicated with the increased PSK modulation order. To recover the carrier frequency by multiplication, a frequency multiplier and divider are needed. For a QPSK signal, a frequency quadrupler and a four times frequency divider are needed. This makes the demodulator more complex and therefore this solution is limited to low modulation order signals.

For high modulation order (more than 4) QAM signals, real-time coherent demodulation is accomplished with a recovered carrier signal. Carrier recovery is commonly implemented in digital signal processing (DSP) platforms on the received intermediated frequency (IF) signals. Limited by the ADC sampling speed, the highest reported single channel data rate in real-time millimeter-wave communication with DSP platforms is below 5.3 Gbps [33]. Paper [C] demonstrates a real-time millimeter-wave communication system with a proposed synchronous baseband receiver. A carrier recovery (CR) subsystem in the receiver is implemented in a digital and analog hybrid way. The received signal is down converted to baseband instead of the IF stage for carrier recovery. Furthermore, the required ADC sampling speed in the proposed CR subsystem is only 100 MSps, which is much lower than previously reported DSP platforms of CR solutions.

Table 4.1 Published real-time transmission experiments over millimetre-wave bands.

Ref	Data rate per channel (Gbps)	Modulation	ADC sampling rate (GSps)	Frequency band	Receiver topology
[34]	22.2	DQPSK	Without DAC	120 GHz	IF (DQPSK)
[62]	8	16-QAM		73.5 GHz	IF (analog PLL)
[23]	42	2-ASK		300 GHz	IF (direct detection)
[20]	2.5	QPSK		87 GHz	Baseband (Costas loop)
[63]	2.5	QPSK	3.52	60 GHz	IF (digital)
[64]	1.5	8-PSK	2	E-Band	IF (digital)
[65]	1.25	16-QAM	0.9375	E-Band	IF (digital)
[66]	1.58	16-QAM	3.456	60 GHz	IF (digital)
[21]	3	16-QAM	3	340 GHz	IF (digital)
[33]	5.3	64-QAM	Not mention	143 GHz	IF (digital)
[19]	5	16-QAM	1.25	E-Band	IF (digital)
This work	**4** **6**	**16-QAM** **QPSK**	**0.1**	**E-Band**	**Baseband (hybrid)**

4.2 Considerations of the pilot tone insertion

In paper [C], the carrier recovery is accomplished with the assistance of a pilot tone. Pilot tone insertion at the transmitter side is a typical solution to relieve the complexity of the receiver synchronization design. As shown in Fig. 4.1, the pilot tone can be inserted at different frequency offsets from the transmitted carrier frequency. There are three examples discussed: the pilot in the center of the carrier, the pilot outside the modulated signal and the pilot embedded in the modulated signal.

In the first case as shown in Fig. 4.1(a), the pilot tone is inserted at the center of the transmitted signal. This can be realized by simply allowing a certain transmitter carrier signal leakage to the RF-port. In the heterodyne receiver, the RF signal is down-converted to an IF frequency. An analog feedforward structure as Fig. 4.1(e) or digital feedforward structure as Fig. 4.1(d) can be used. As an example, an analog feedforward structure is proposed in [67] which uses injection locking to extract the pilot tone, and then the pilot tone is utilized for carrier recovery and demodulation. In a homodyne receiver, this pilot tone will be down-converted close to DC. Most of the high-speed ADC requires AC-coupled input thus it is difficult to sample this pilot which is close to the DC.

In addition, the pilot tone as described in Fig. 4.1(b) can be inserted outside the signal band. In this case, it can be easily filtered out by a narrow band pass filter, and then be used for carrier recovery or phase noise mitigation. The drawback of this method is the spectrum efficiency degradation due to extra bandwidth needed in addition to the signal band. The feedback structure is shown in Fig. 4.1(f) can be used in this case. The feedback loop can be realized with both analog and digital solutions. After the pilot tone has been extracted, it is used to adjust the LO frequency in the receiver.

As another alternative depicted in Fig. 4.1(c), the pilot tone is inserted in-band regarding the transmitted data. In this way, the spectrum efficiency remains the same as the case without the pilot. On the other hand, the power of the pilot tone needs to be adjusted carefully, so that the pilot tone has little impact on the quality of the transmission signal. The structure shown in Fig. 4.1(f) could be applied in this case to extract the pilot. Furthermore, in a homodyne receiver, the pilot tone in the third case is closer to the DC than the second case, which allows a lower sampling rate for the ADC and DAC in the DSP platform.

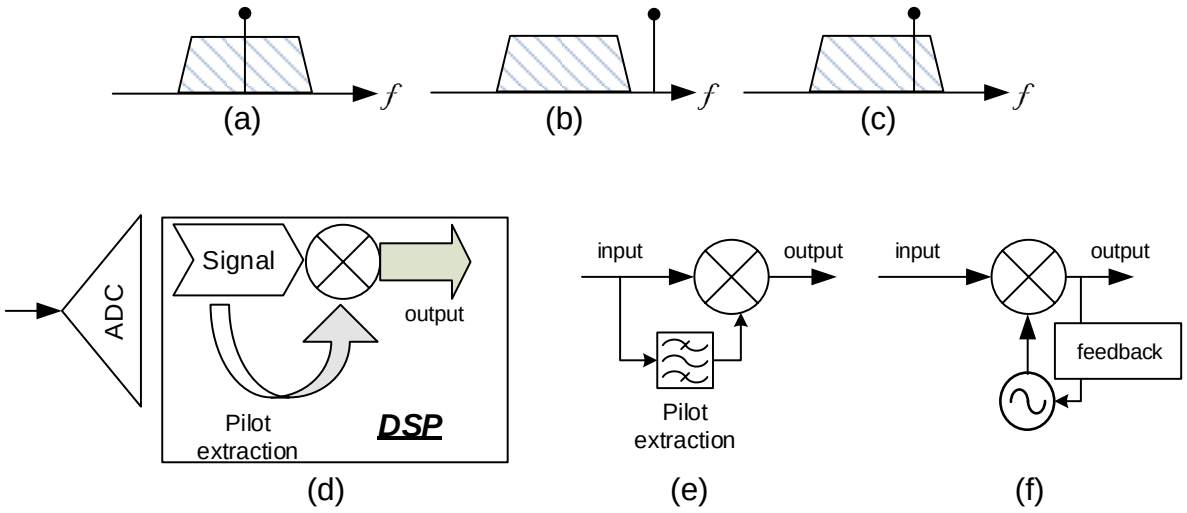

Fig. 4.1. Choice of pilot tone insertion: (a) carrier frequency pilot; (b) out-of-band pilot tone; (c) in-band pilot tone. Pilot extraction methods: (d) full digital feedforward; (e) analog feed forward; (f) analog feedback

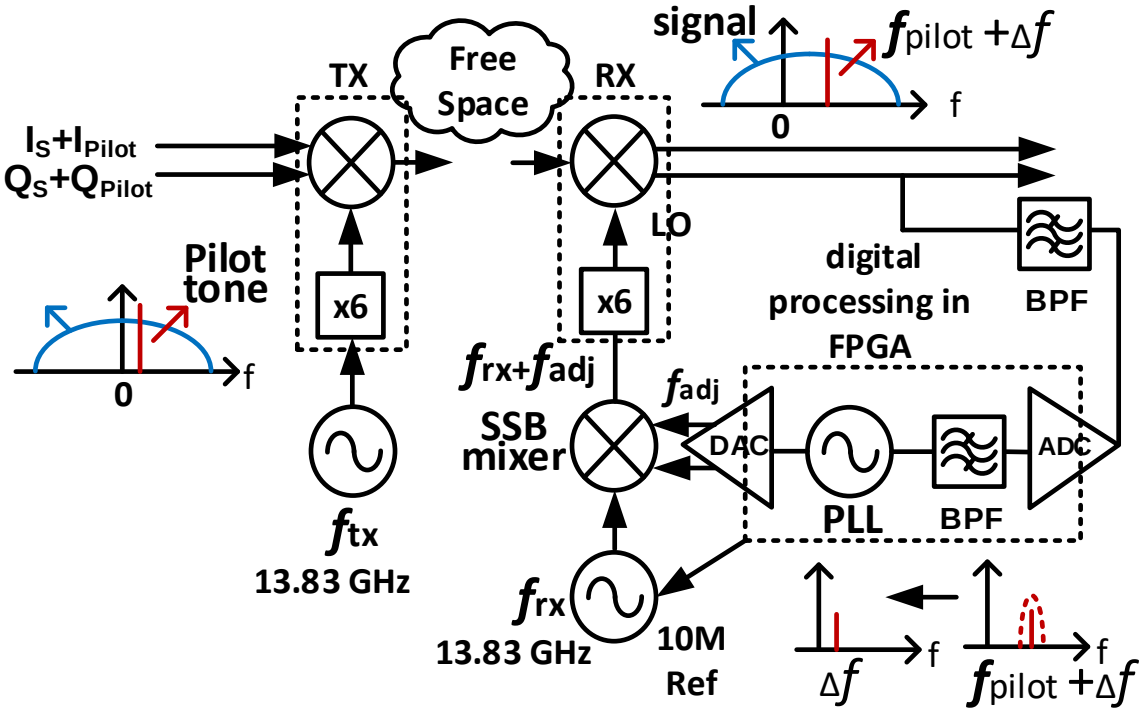

Fig. 4.2 Proposed E-band link structure.

4.3 The proposed millimeter-wave communication system

An E-band communication system structure is proposed and shown in Fig. 4.2. At the transmitter side, a pilot tone is superimposed within the signal band as the third case discussed in the last section. The pilot tone is upconverted to E-band together with the signal using an E-band TX module. At the receiver side, the received signal is down-converted to the baseband by an E-band RX module. There is a frequency offset remained with the baseband signal due to the frequency difference of two separate LOs in the transmitter side and the receiver side. A

CR subsystem is proposed to remove the frequency offset. This CR subsystem includes a DSP platform and analog components. In the DSP platform, the pilot tone is extracted from the baseband signal and helps to identify the frequency offset. Then the LO frequency is adjusted accordingly by analog components to remove the frequency offset.

The pilot tone is chosen to be close to the DC. At the receiver side, it can be extracted by a DSP platform with low-speed ADCs and DACs. The power of the pilot tone needs to be chosen carefully since it will introduce unwanted intermodulation signals. Meanwhile, the power of the pilot tone has to be large enough to be detected on the receiver side.

4.4 Carrier recovery subsystem

A novel carrier recovery principle is proposed in paper [C]. The frequency of the pilot tone f_{pilot} has a fixed relationship with the transmitter LO frequency as $f_{pilot} = f_{tx}/N$. As shown in Fig. 4.2, there is a six times frequency multiplier in the E-band module in both the transmitter side and the receiver side. The carrier frequency in the transmitter and the receiver are denoted $6 \times f_{tx}$ and $6 \times f_{rx}$, respectively. After the received signal is down converted to the baseband, the received pilot signal is $f_{pilot} + 6 \times (f_{tx} - f_{rx}) = f_{pilot} + \Delta f$. This signal is sampled and send into the DSP platform which shares a reference clock with the receiver LO. In this DSP platform, the received pilot signal $f_{pilot} + \Delta f$ is multiplied with the 1/N times of receiver LO frequency f_{rx} to find out the frequency offset. Then the phase-locked loop (PLL) in the DSP platform generates an adjustment signal accordingly. The adjustment signal is converted to an analog signal and mixed with the original LO signal by a single side band (SSB) mixer. This mixed signal $f_{rx} + f_{adj}$ becomes the new LO. When $f_{adj} = f_{rx} - f_{tx}$, the CR loop will converge and the received pilot signal becomes $f_{pilot} = (f_{rx} + f_{adj})/N$.

The detailed block diagram of the carrier recovery implementation is shown in Fig. 4.3. The pilot tone frequency is set to 21 MHz which can be sampled by a 100 MSps ADC. The received signal passes through a surface acoustic wave (SAW) bandpass filter (BPF) to extract the pilot signal. Then the received pilot signal is digitalized by a 100 MSps ADC and sent into an FPGA running at 200 MHz which is fully synchronized with the receiver LO. A 30 tap digital BPF is used to further improve the pilot signal's quality. There are two numerical controlled oscillators (NCOs) in the FPGA. NCO1 is used to provide a digital copy of f_{rx}. NCO2 is a tuneable oscillator which provides the adjustment signal f_{adj}. By summing up the outputs of two NCOs, a replica of the SSB mixer output $f_{rx} + f_{adj}$ is created. It is divided by N in order to extract the frequency difference with the received pilot signal utilizing a phase detector. The phase detector consists of a digital mixer and a loop filter. If the received pilot tone is outside the BPF, the NCO2 will sweep the frequency until the pilot tone is captured.

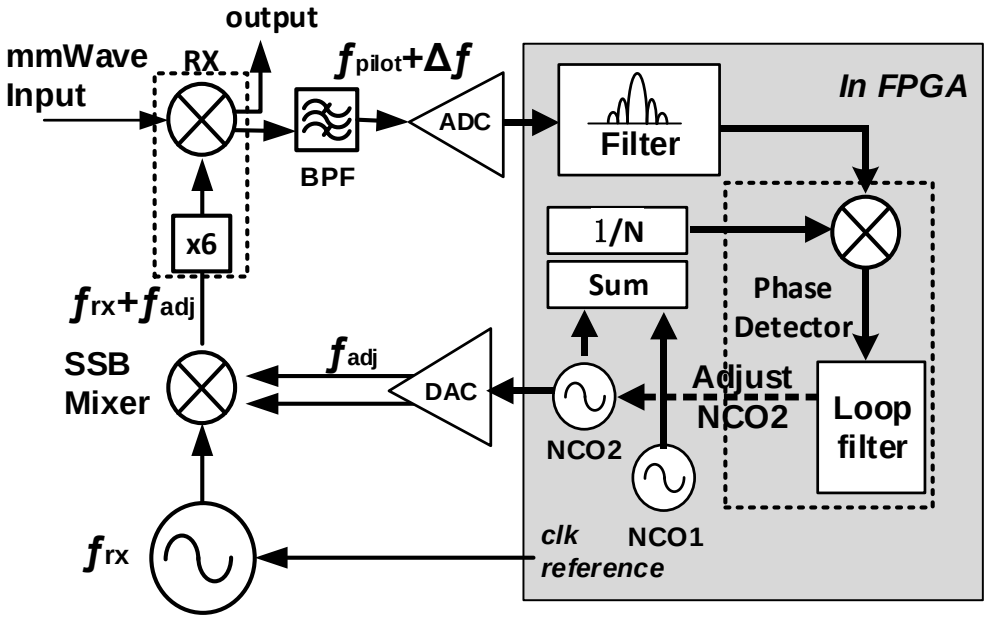

Fig. 4.3 Block diagram of the synchronous baseband receiver.

4.5 Performance verification

To verify the performance of the proposed synchronous baseband receiver, two commercial E-band frontend modules from SiversIMA are used. The E-band transmitter and receiver modules are connected by a waveguide and a 30-dB attenuator. The LO frequency is set at 13.83 GHz, after six times multiplication, the carrier frequency becomes 83 GHz. An oscilloscope is used to observe the constellation diagram and estimate the BER of the recovered signal.

This E-band communication link has successfully transmitted a 4 Gbps 16-QAM signal and a 6 Gbps QPSK signal. The proposed synchronous baseband receiver is verified at 3 MHz frequency offset. The constellation of the received 4 Gbps 16-QAM signal and a 6 Gbps QPSK signal are shown in Fig. 4.4 without any equalization applied. The estimated BER from the constellations are 2.02×10^{-7} and 2.18×10^{-7}, respectively. The power ratio between the pilot tone and the signal is -40 dB.

Different power ratios between the pilot and the signal are also studied in 6 Gbps QPSK transmissions. The power ratio is varied from -60 dB to -20 dB. The minimum power ratio that maintains the functional CR system is -40 dB. Fig. 4.5 shows different receiving BER while varying the power ratio.

The data rate is at the moment limited by the intermodulation introduced by the pilot tone. The intermodulation brings the amplitude fluctuation to the signal, which increases EVM. A figure of the EVM versus different power ratios between the pilot and a 16-QAM signal is shown in Fig. 4.6. At a ratio of -40 dB, the intermodulation will increase the EVM with 1%. The power of the pilot signal cannot be lower than -40 dB according to the measurement. Otherwise, the pilot signal cannot be extracted at the receiver.

For a 1 Gbaud signal, if the power ratio between the pilot and the baseband signal is -40 dB, the bandwidth of the BPF in the receiver is 10 kHz, the pilot signal's SNR after the BPF is

$$-40 + 10lg\frac{10^9}{10^4} = 10\ dB. \tag{4.1}$$

To further increase of the data rate, the power ratio between the pilot and the signal needs to be lower. Instead of using a CW signal, a PRBS can be used as the pilot signal. By doing the correlation in the receiver with the same PRBS, the pilot's power is accumulated. If the symbol rate of the PRBS is 1 Mbaud, the length of the sequence is 1000, to have a 10 dB SNR for the pilot signal in the receiver, the power ratio between the pilot and the baseband signal is

$$\frac{P_{PN}}{P_{BS}} = 10 - 10\text{lg}1000 - 10\,\text{lg}\left(\frac{10^9}{10^6}\right) = -20 - 30 = -50\ \text{dB}. \tag{4.2}$$

By using this PRBS signal, a power ratio of -50 dB between the pilot and the baseband signal is enough for the CR loop. The power of the pilot tone is 10 dB less in this case which decrease the interference to the baseband signal, thus a higher data rate can be expected.

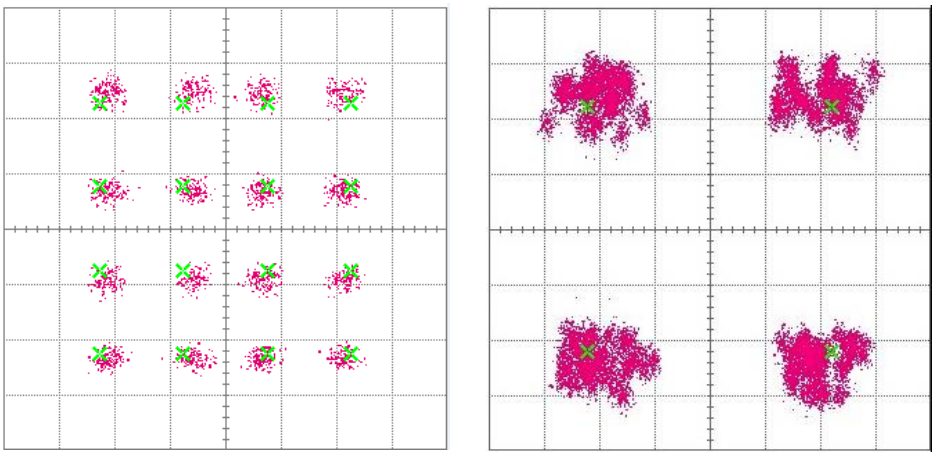

(a) 4 Gbps 16-QAM (b) 6 Gbps QPSK

Fig. 4.4 Constellations of the received signals.

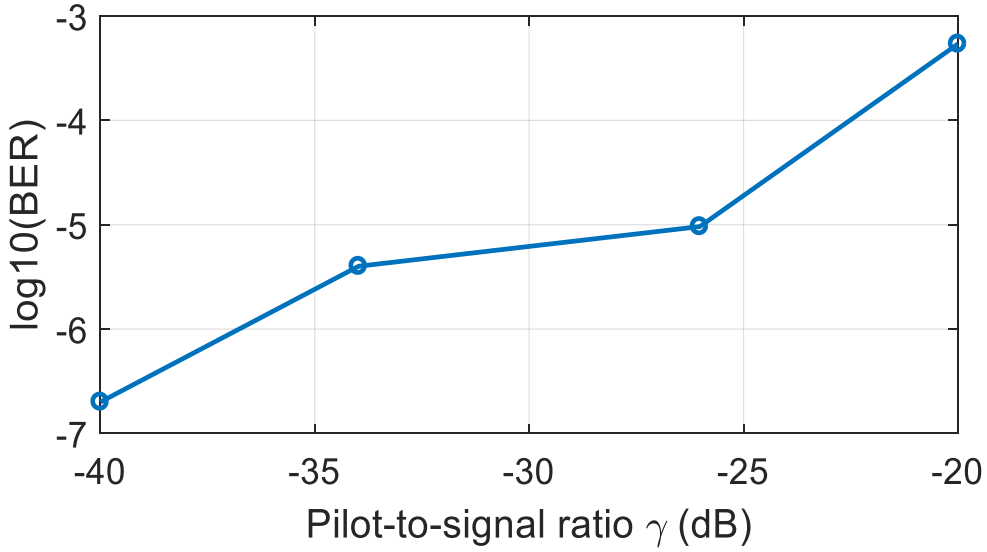

Fig. 4.5 BER versus power ratio γ for 6 Gbps QPSK transmission

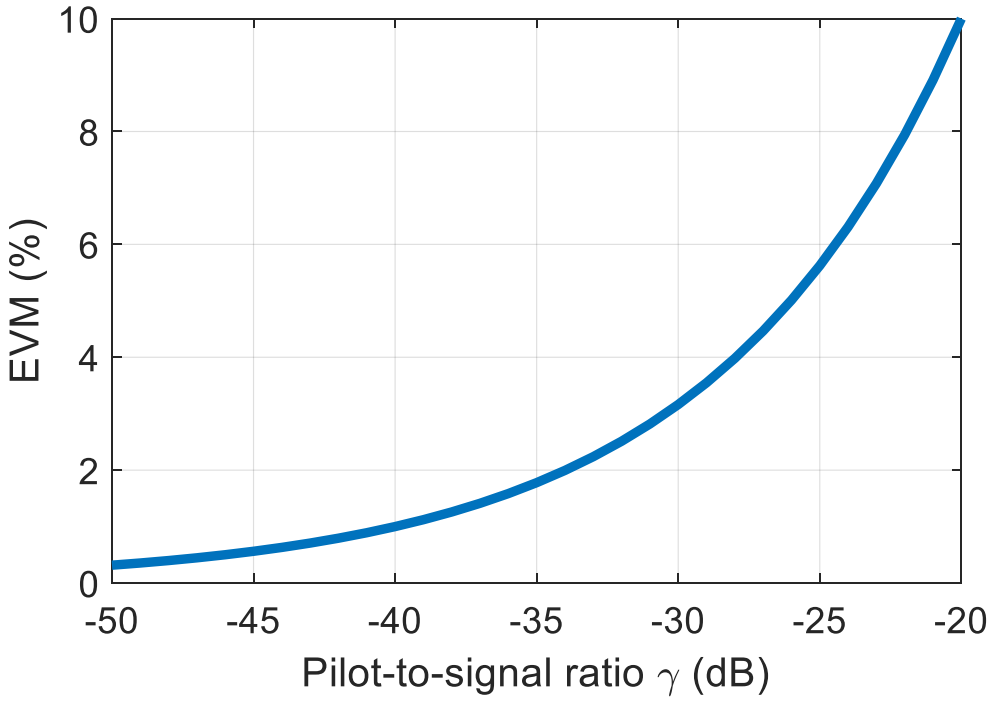

Fig. 4.6 Simulated EVM versus power ratio γ between the pilot and the signal.

Chapter 5

Conclusions and future work

Driven by the rapid development of high data rate communications, the requirements on the capacity of communication links are increasing dramatically. In this thesis, challenges in the implementation of high data rate communication at millimeter-wave frequencies are addressed and solutions are provided. According to the Shannon theorem, the capacity of a noisy communication channel is limited by the available bandwidth and the signal to noise ratio, and the signal to noise ratio limits the spectrum efficiency of communication channels. As a conclusion, either increasing the available bandwidth or the spectrum efficiency could lead to increased capacity.

Frequency bands over millimeter-wave offer large bandwidth from several GHz to tens of GHz, therefore the opportunities to achieve high data rate communications. In this case, wide-band modems are needed to support high data rate modulation and demodulation. In chapter 2, a 40 Gbps DQPSK modem solution is proposed aiming to be integrated with the D-band frontend modules published in [1] with a bandwidth more than 40 GHz. The differential encoder and detector are the key components in this DQPSK modem. The differential encoder is realized in a single FPGA, while the differential detector is realized by analog components. The modem has been verified at 40 Gbps.

To maintain a high signal-to-noise ratio at millimeter-wave frequencies and higher is challenging due to the difficulty in high-frequency signal generation with high output power. In addition, it is important to avoid non-linear distortion of the power amplifiers. As a result, the transmitter needs to back off several dB of output power in order to maintain the signal quality. In chapter 3, a novel symbol-based outphasing power combining transmitter is demonstrated at E-band with commercially available components. This E-band system supports signal transmission at the maximum output power of the power amplifier without suffering from non-linear distortions. Unlike the conventional outphasing transmitter which implements the outphasing with the IF signal by using analog circuit, the proposed outphasing transmitter implements the outphasing digitally on symbols, which simplify the implementation. To the best of the authors' knowledge, this works exhibits the highest transmission data rate at the highest carrier frequency in an outphasing power combining system.

To achieve high spectrum efficiency in communication systems, high order modulation signal such as QAM signals are commonly used. However, at the receiver side, coherent detection is needed to demodulate high order QAM signals. In chapter 4, a synchronous baseband receiver is proposed with a carrier recovery subsystem. A pilot tone is inserted in-band at the transmitter side to assist the receiver to recover the carrier frequency. The carrier recovery subsystem is realized in a hybrid analog and digital solution. The required ADC sampling rate is only 100 MSps. The proposed receiver is verified in an E-band link with a 4 Gbps 16-QAM signal and a 6 Gbps QPSK signal. Compared with the recent publication on real-time transmission shown in Table 4.1, the proposed receiver is the only modulation independent baseband receiver with the lowest ADC sampling rate.

For future plans, the proposed DQPSK modem in [A] could be further investigated together with the D-band frontend module as a real-time communication link. It is also interesting to test the CR subsystem proposed in [C] together with a D-band communication link. A PRBS signal can be used as a pilot to further increase the data rate.

Acknowledgment

I would like to take this opportunity to express my gratitude to the people who have supported me throughout my studies.

First of all, I would like to thank my main supervisor and examiner Prof. Herbert Zirath for giving me this great opportunity to work in MEL as a PhD student. I am grateful for all the support and the guidance that he gave. His rigorous attitude and enthusiasm for scientific research inspired me to take my work forward. I would also like to thank my co-supervisor Dr. Zhongxia Simon He for his valuable help in both my work and life. It was him who spent a lot of time teaching me how to do research from the very beginning and helped me to adapt the life in Sweden. Thanks for all the encouragement and support that he gave. I appreciate that he always being available when I need help. I wish to thank my co-supervisor Dr. Yinggang Li for his expert advice and feedbacks.

I would like to thank my friend and co-worker Dr. Jingjing Chen for her valuable suggestions, fruitful discussion and so much help with the measurement and writing. I am grateful that she always being such supportive and kind. I also owe my thanks to all my colleagues for creating such a pleasant environment to work with you. I would like to thank my friend Aimin Wang for her caring and encouragement.

Last but not least, I want to thank my family for their unconditional love, greatest support and faith in me.

This research was financed by the Swedish Foundation for Strategic Research High-speed wireless communication project (SSF Trådlös kommunikation 100G).

References

[1] S. Carpenter, Z. He, M. Bao and H. Zirath, "A Highly Integrated Chipset for 40 Gbps Wireless D-Band Communication Based on a 250 nm InP DHBT Technology," 2014 IEEE Compound Semiconductor Integrated Circuit Symposium (CSICS), La Jolla, CA, 2014, pp. 1-4.

[2] J. Gantz, and D. Reinsel, "The digital universe in 2020: Big data, bigger digital shadows, and biggest growth in the far east," IDC iView: IDC Analyze the future 2007, no. 2012, pp. 1-16, February 2013.

[3] "Ericsson mobility report," June, 2018.

[4] P. Sharma, "Evolution of mobile wireless communication networks-1G to 5G as well as future prospective of next generation communication network." International Journal of Computer Science and Mobile Computing, vol. 2, pp. 47-53, August 2013.

[5] M. I. Baba, N. Nafees, I. Manzoor, K. A. Naik, and S. Ahmed, "Evolution of Mobile Wireless Communication Systems from 1G to 5G: A Comparative Analysis," in International Journal of Scientific Research in Computer Science, Engineering and Information Technology, vol. 4, issue 1, April 2018.

[6] A. U. Gawas, "An overview on evolution of mobile wireless communication networks: 1G-6G," International Journal on Recent and Innovation Trends in Computing and Communication, vol. 3, no. 5, pp. 3230-3133, May 2015.

[7] "To be first in 5G, first get to the core, " Ericsson, 2018.

[8] T. S. Rappaport, S. Sun, R. Mayzus, H. Zhao, Y. Azar, K. Wang, G. N. Wong, J. K. Schulz, M. Samimi, and F. Gutierrez, "Millimeter-wave Mobile Communications for 5G Cellular: It Will Work," in IEEE Access, vol. 1, pp. 335-349, 2013.

[9] "5G deployment considerations, " Ericsson, 2018.

[10] "Ericsson White paper, " January, 2017.

[11] "Ericsson microwave outlook, " December, 2017.

[12] M. Jaber, M. A. Imran, R. Tafazolli and A. Tukmanov, "5G Backhaul Challenges and Emerging Research Directions: A Survey," in IEEE Access, vol. 4, pp. 1743-1766, 2016.

[13] J. R. Pierce, "Symbol signal and noise," 1961.

[14] C. E. Shannon, "A mathematical theory of communication," in The Bell System Technical Journal, vol. 27, no. 4, pp. 623-656, Oct. 1948.

[15] J. Wells, "Faster than fiber: The future of multi-G/s wireless," in IEEE Microwave Magazine, vol. 10, no. 3, pp. 104-112, May 2009.

[16] D. Lopez-Diaz, A. Tessmann, A. Leuther, S. Wagner, M. Schlechtweg, O. Ambacher, S. Koenig et al. "A 240 GHz quadrature receiver and transmitter for data transmission up to 40 Gbit/s." In Microwave Conference (EuMC), 2013 European, pp. 1411-1414. IEEE, 2013.

[17] H. Hamada, T. Fujimura, I. Abdo, K. Okada, H. J. Song, H. Sugiyama, H. Matsuzaki, and H. Nosaka, "300-GHz. 100-Gb/s InP-HEMT Wireless Transceiver Using a 300-GHz Fundamental Mixer," 2018 IEEE/MTT-S International Microwave Symposium - IMS, Philadelphia, PA, 2018, pp. 1480-1483.

[18] J. Chen, D. Kuylenstierna, S. E. Gunnarsson, Z. S. He, T. Eriksson, T. Swahn and H. Zirath, "Influence of White LO Noise on Wideband Communication," in IEEE Transactions on Microwave Theory and Techniques, vol. 66, no. 7, pp. 3349-3359, July 2018.

[19] Z. He, J. Chen, C. Svensson, L. Bao, A. Rhodin, Y. Li, J. An and H. Zirath, "A Hardware Efficient Implementation of a Digital Baseband Receiver for High-Capacity Millimeter-Wave Radios," in IEEE Transactions on Microwave Theory and Techniques, vol. 63, no. 5, pp. 1683-1692, May 2015.

[20] S. Huang, Y. Yeh, H. Wang, P. Chen and J. Lee, "W-Band BPSK and QPSK Transceivers with Costas-Loop Carrier Recovery in 65-nm CMOS Technology," in IEEE Journal of Solid-State Circuits, vol. 46, no. 12, pp. 3033-3046, December 2011.

[21] C. Wang , B. Lu, C. Lin, Q. Chen, L. Miao, X. Deng and J. Zhang, "0.34-THz Wireless Link Based on High-Order Modulation for Future Wireless Local Area Network Applications," in IEEE Transactions on Terahertz Science and Technology, vol. 4, no. 1, pp. 75-85, Jan. 2014.

[22] P. Rodríguez-Vázquez, J. Grzyb, N. Sarmah, B. Heinemann and U. R. Pfeiffer, "A 65 Gbps QPSK one meter wireless link operating at a 225–255 GHz tunable carrier in a SiGe HBT technology," 2018 IEEE Radio and Wireless Symposium (RWS), Anaheim, CA, 2018, pp. 146-149.

[23] T. Nagatsuma, "Breakthroughs in Photonics 2013: THz Communications Based on Photonics," in IEEE Photonics Journal, vol. 6, no. 2, pp. 1-5, April 2014, Art no. 0701505.

[24] S. Carpenter, D. Nopchinda, M. Abbasi, Z. S. He, M. Bao, T. Eriksson and H. Zirath, "A D-Band 48-Gbit/s 64-QAM/QPSK Direct-Conversion I/Q Transceiver Chipset," in IEEE Transactions on Microwave Theory and Techniques, vol. 64, no. 4, pp. 1285-1296, April 2016.

[25] H. Song, J. Kim, K. Ajito, N. Kukutsu and M. Yaita, "50-Gb/s Direct Conversion QPSK Modulator and Demodulator MMICs for Terahertz Communications at 300 GHz," in IEEE Transactions on Microwave Theory and Techniques, vol. 62, no. 3, pp. 600-609, March 2014.

[26] I. Kallfass , J. Antes, T. Schneider, F. Kurz, D. Lopez-Diaz, S. Diebold, H. Massler, A. Leuther and A. Tessmann, "All Active MMIC-Based Wireless Communication at 220

GHz," in IEEE Transactions on Terahertz Science and Technology, vol. 1, no. 2, pp. 477-487, November 2011.

[27] I. Ando, M. Tanio, M. Ito, T. Kuwabara, T. Marumoto and K. Kunihiro, "Wireless D-band communication up to 60 Gbit/s with 64QAM using GaAs HEMT technology," 2016 IEEE Radio and Wireless Symposium (RWS), Austin, TX, 2016, pp. 193-195.

[28] K. Katayama, K. Takano, S. Amakawa, S. Hara, T. Yoshida and M. Fujishima, "CMOS 300-GHz 64-QAM transmitter," 2016 IEEE MTT-S International Microwave Symposium (IMS), San Francisco, CA, 2016, pp. 1-4.

[29] F. Boes, T. Messinger, J. Antes, D. Meier, A. Tessmann, A. Inam and I. Kallfass, "Ultra-broadband MMIC-based wireless link at 240 GHz enabled by 64GS/s DAC," 2014 39th International Conference on Infrared, Millimeter, and Terahertz waves (IRMMW-THz), Tucson, AZ, 2014, pp. 1-2.

[30] C. Lin, B. Lu, C. Wang and Q. Wu, "A 2×40 Gbps wireless communication system using 0.14 THz band oritho-mode transducer," 2015 40th International Conference on Infrared, Millimeter, and Terahertz waves (IRMMW-THz), Hong Kong, 2015, pp. 1-2.

[31] K. Katayama , K. Takano, S. Amakawa, S. Hara, A. Kasamatsu, K. Mizuno, K. Takahashi, T. Yoshida and M. Fujishima, "A 300 GHz CMOS Transmitter With 32-QAM 17.5 Gb/s/ch Capability Over Six Channels," in IEEE Journal of Solid-State Circuits, vol. 51, no. 12, pp. 3037-3048, Dec. 2016.

[32] H. Hamada, T. Fujimura, I. Abdo, K. Okada, H. J. Song, H. Sugiyama, H. Matsuzaki and H. Nosaka, "300-GHz. 100-Gb/s InP-HEMT Wireless Transceiver Using a 300-GHz Fundamental Mixer," 2018 IEEE/MTT-S International Microwave Symposium - IMS, Philadelphia, PA, 2018, pp. 1480-1483.

[33] V. Vassilev, Z. S. He, S. Carpenter, H. Zirath, Y. Yan, A. Hassona, M. Bao, T. Emanuelsson, J. Chen, M. Horberg, Y. Li and J. Hansrydl, "Spectrum Efficient D-band Communication Link for Real-time Multi-gigabit Wireless Transmission," 2018 IEEE/MTT-S International Microwave Symposium - IMS, Philadelphia, PA, 2018, pp. 1523-1526.

[34] H. Takahashi, A. Hirata, J. Takeuchi, N. Kukutsu, T. Kosugi and K. Murata, "120-GHz-band 20-Gbit/s transmitter and receiver MMICs using quadrature phase shift keying," 2012 7th European Microwave Integrated Circuit Conference, Amsterdam, 2012, pp. 313-316.

[35] K. K. Tokgoz, S. Maki, J. Pang, N. Nagashima, I. Abdo, S. Kawai, T. Fujimura, Y. Kawano, T. Suzuki, T. Iwai and K. Okada, "A 120Gb/s 16QAM CMOS millimeter-wave wireless transceiver," 2018 IEEE International Solid - State Circuits Conference - (ISSCC), San Francisco, CA, 2018, pp. 168-170.

[36] Z. He, D. Nopchinda, T. Swahn and H. Zirath, "A 15-Gb/s 8-PSK Demodulator With Comparator-Based Carrier Synchronization," in IEEE Transactions on Microwave Theory and Techniques, vol. 63, no. 8, pp. 2630-2637, Aug. 2015.

[37] Z. He, J. Chen, Y. Li and H. Zirath, “A Novel FPGA-Based 2.5 Gbps DQPSK Modem for High Capacity Microwave Radios”, IEEE International Conference on Communications (ICC), 2010, pp. 1-4, May 2010.

[38] Z. He, W. Wu, J. Chen, Y. Li, D. Stackenas and H. Zirath, “An FPGA-based 5 Gbit/s D-QPSK Modem for E-band Point-to-Point Radios”, European Microwave Integrated Circuits Conference (EuMIC) 2011, pp. 690-692, September 2011.

[39] J. Chen, Z. He, Y. Li, T. Swahn and H. Zirath, “A data-rate adaptable modem solution for millimeter-wave wireless fronthaul networks,” in IEEE International Conference on Communication Workshop (ICCW), London, 2015, pp. 1-6.

[40] S. Masuda, T. Ohki, K. Makiyama, M. Kanamura, N. Okamoto, H. Shigematsu, K. Imanishi, T. Kikkawa, K. Joshin, and N. Hara, "GaN MMIC amplifiers for W-band transceivers," 2009 European Microwave Integrated Circuits Conference (EuMIC), Rome, 2009, pp. 443-446.

[41] M. Micovic, A. Kurdoghlian, K. Shinohara, S. Burnham, I. Milosavljevic, M. Hu, A. Corrion, A. Fung, R. Lin, L. Samoska and P. Kangaslahti, "W-Band GaN MMIC with 842 mW output power at 88 GHz," 2010 IEEE MTT-S International Microwave Symposium, Anaheim, CA, 2010, pp. 237-239.

[42] A. Brown, K. Brown, J. Chen, K. C. Hwang, N. Kolias and R. Scott, "W-band GaN power amplifier MMICs," 2011 IEEE MTT-S International Microwave Symposium, Baltimore, MD, 2011, pp. 1-4.

[43] M. Micovic, A. Kurdoghlian, A. Margomenos, D. F. Brown, K. Shinohara, S. Burnham, I. Milosavljevic, R. Bowen, A.J. Williams, P. Hashimoto, R. Grabar, C. Butler, A. Schmitz, P. J. Willadsen and D. H. Chow, "92–96 GHz GaN power amplifiers," 2012 IEEE/MTT-S International Microwave Symposium Digest, Montreal, QC, 2012, pp. 1-3.

[44] J. Schellenberg, B. Kim and T. Phan, "W-Band, Broadband 2W GaN MMIC," 2013 IEEE MTT-S International Microwave Symposium Digest (MTT), Seattle, WA, 2013, pp. 1-4.

[45] D. Schwantuschke, B. J. Godejohann, S. Breuer, P. Bruckner, M. Mikulla, R. Quay and O. Ambacher, "Broadband E-Band Power Amplifier MMIC Based on an AlGaN/GaN HEMT Technology with 30 dBm Output Power," 2016 IEEE Compound Semiconductor Integrated Circuit Symposium (CSICS), Austin, TX, 2016, pp. 1-4.

[46] S. Wu, F. Guo, J. Gao, W. Wang, Z. Li, N. Huang and T. Chen, "W-band AlGaN/GaN MMIC PA with 3.1W output power," 2017 14th China International Forum on Solid State Lighting: International Forum on Wide Bandgap Semiconductors China (SSLChina: IFWS), Beijing, 2017, pp. 219-223.

[47] Z. Xu, Q. J. Gu and M. F. Chang, "A Three Stage, Fully Differential 128–157 GHz CMOS Amplifier with Wide Band Matching," in IEEE Microwave and Wireless Components Letters, vol. 21, no. 10, pp. 550-552, Oct. 2011.

[48] Z. Tsai, H. Liao, Y. Hsiao, H. Wang, J. Liu, M. F. Chang, Y. Teng and G. Huang, "A 1.2V broadband D-band power amplifier with 13.2-dBm output power in standard RF 65-nm

CMOS," 2012 IEEE/MTT-S International Microwave Symposium Digest, Montreal, QC, 2012, pp. 1-3.

[49] H. Takahashi, T. Kosugi, A. Hirata, J. Takeuchi, K. Murata and N. Kukutsu, "120-GHz-Band Fully Integrated Wireless Link Using QSPK for Realtime 10-Gbit/s Transmission," in IEEE Transactions on Microwave Theory and Techniques, vol. 61, no. 12, pp. 4745-4753, Dec. 2013.

[50] H. Yanfei, Y. Weihua, L. Xiaobin, L. Yuanjie, D. Shaobo and F. Zhihong, "Design of power amplifier MMICs based on GaN HEMTs at 110GHz," 2015 Asia-Pacific Microwave Conference (APMC), Nanjing, 2015, pp. 1-3.

[51] A. Ali, E. Cipriani, T. K. Johansen and P. Colantonio, "Study of 130 nm SiGe HBT Periphery in the Design of 160 GHz Power Amplifier," 2018 First International Workshop on Mobile Terahertz Systems (IWMTS), Duisburg, 2018, pp. 1-5.

[52] Y. J. Seong, C. S. Cho and J. W. Lee, "Digital pre-distortion architecture for RF power amplifier based on affine projection algorithm," in Electronics Letters, vol. 48, no. 15, pp. 947-948, July 19 2012.

[53] P. Sojoodi Sardrood, G. R. Solat and V. Taba taba vakili, "Improvement eye diagram opening by base band pre-distortion over nonlinear channel in DVB-RCS transmitter," International Congress on Ultra Modern Telecommunications and Control Systems, Moscow, 2010, pp. 26-30.

[54] H.Chireix, "High Power Outphasing Modulation," in Proceedings of the Institute of Radio Engineers, vol. 23, no. 11, pp. 1370-1392, Nov. 1935.

[55] D. Cox, "Linear Amplification with Nonlinear Components," in IEEE Transactions on Communications, vol. 22, no. 12, pp. 1942-1945, Dec 1974.

[56] M. S. Mehrjoo and J. F. Buckwalter, "A Differential Oscillator Injection Locking Technique for an 8 GHz Outphasing Modulator With 22.7% Modulation Efficiency," in IEEE Journal of Solid-State Circuits, vol. 51, no. 12, pp. 3093-3102, Dec. 2016.

[57] C. Xie, D. Cripe, J. Reyland, D. Landt and A. Walker, "Development of High-Efficiency X-Band Outphasing Transmitter," 2014 IEEE Compound Semiconductor Integrated Circuit Symposium (CSICS), La Jolla, CA, 2014, pp. 1-4.

[58] M. S. Mehrjoo, S. Zihir, G. M. Rebeiz and J. F. Buckwalter, "A 1.1-Gbit/s 10-GHz Outphasing Modulator With 23-dBm Output Power and 60-dB Dynamic Range in 45-nm CMOS SOI," in IEEE Transactions on Microwave Theory and Techniques, vol. 63, no. 7, pp. 2289-2300, July 2015.

[59] C. Liang and B. Razavi, "Transmitter Linearization by Beamforming," in IEEE Journal of Solid-State Circuits, vol. 46, no. 9, pp. 1956-1969, Sept. 2011

[60] D. Zhao, S. Kulkarni and P. Reynaert, "A 60-GHz Outphasing Transmitter in 40-nm CMOS," in IEEE Journal of Solid-State Circuits, vol. 47, no. 12, pp. 3172-3183, Dec. 2012.

[61] A. Ç. Ulusoy and H. Schumacher, "Multi-Gb/s Analog Synchronous QPSK Demodulator with Phase-Noise Suppression," in IEEE Transactions on Microwave Theory and Techniques, vol. 60, no. 11, pp. 3591-3598, Nov. 2012.

[62] P. Harati, A. Dyskin and I. Kallfass, "Analog Carrier Recovery for Broadband Wireless Communication Links," 2018 48th European Microwave Conference (EuMC), Madrid, Spain, 2018, pp. 1401-1404.

[63] T. Tsukizawa, "A fully integrated 60-GHz CMOS transceiver chipset based on WiGig/IEEE 802.11ad with built-in self calibration for mobile usage", IEEE J. Solid-State Circuits, vol. 48, no. 12, pp. 3146-3159, Dec. 2013.

[64] V. Dyadyuk, "A multigigabit millimeter-wave communication system with improved spectral efficiency", in IEEE Transactions on Microwave Theory and Techniques., vol. 55, no. 12, pp. 2813-2821, Dec. 2007.

[65] M. S. Kang, B. S. Kim, K. S. Kim, W. J. Byun, H. C. Park, "16-QAM-based highly spectral-efficient e-band communication system with bit rate up to 10 Gbit/s", ETRI J., vol. 34, no. 5, pp. 649-654, Oct. 2012.

[66] K. Okada, "A full four-channel 6.3-Gb/s 60-GHz CMOS transceiver with low-power analog and digital baseband circuitry", IEEE J. Solid-State Circuits, vol. 48, no. 1, pp. 46-65, Jan. 2013.

[67] Z. He, D. Kuylenstierna, S. Lai and H. Zirath, "A 12 Gbps analog QPSK baseband receiver based on injection-locked VCO," 2015 IEEE MTT-S International Microwave Symposium, Phoenix, AZ, 2015, pp. 1-4.

Paper A

A 40 Gbps DQPSK modem for millimeter-wave communications

S. An, J. Chen, Z. He, S. Wang and H. Zirath

Asia-Pacific Microwave Conference (APMC), Nanjing, 2015, pp. 1-3.

Paper B

An 8 Gbps E-band QAM transmitter using symbol-based outphasing power combining technique

S. An, Z. S. He, J. Chen, Y. Li and H. Zirath

2017 IEEE International Symposium on Radio-Frequency Integration Technology (RFIT), Seoul, 2017, pp. 150-152.

Paper C

A synchronous baseband receiver for high data rate millimeter-wave communication systems

S. An, Z. He, J. Chen, H. Han, H. Zirath

Submitted to *IEEE Microwave and Wireless Components Letters*.